OPTIMIZATION OF DISCONTINUOUS DYNAMIC SYSTEMS

P. I. Barton
Department of Chemical Engineering and Energy Laboratory
Massachusetts Institute of Technology, Cambridge, MA 02139

J. R. Banga
Chemical Engineering Laboratory, IIM-CSIC, 36208 Vigo, Spain

S. Galán
Departmento de Ingeniría Química, Universidad Politécnica de Madrid, 28006 Madrid, Spain

ABSTRACT

The optimization of discontinuous (or hybrid) dynamic systems is considered. In particular, the potential of numerical optimization procedures to make optimal sequencing decisions in hybrid dynamic systems is explored. A general formulation for hybrid optimal control is presented. Further analysis yields a nonsmooth formulation for parameter optimization of hybrid dynamic systems, which may also be used to approximate optimal control problems. For illustration, the design of a minimum time changeover operation for a pressure vessel avoiding the formation of explosive mixtures is considered. Results show that a direct stochastic search procedure can indeed make the sequencing decisions automatically given merely a statement of the system model and the path and point constraints.

INTRODUCTION

A large number of engineering tasks can be formulated as open loop optimal control problems, where we search a priori for the input profiles to a dynamic system that optimize a given performance measure over a finite time interval. Continuous optimal control problems have received extensive theoretical and numerical treatment in the literature (e.g., [1, 2]), and these treatments in principle extend to problems in which there are discontinuities due to bounds on the control profiles or sequences of inequality path constraint activations and/or deactivations along the optimal trajectory.

However, many dynamic systems experience significant additional discontinuities during transients of engineering interest. For example, the start-up of a chemical plant will require a sequence of discrete control actions, such as starting/stopping pumps or the action of an interlock system, and during such transients transitions in the physical regime such as flow reversals/transitions or (thermodynamic) phase changes are highly likely to occur. These latter phenomena are often modeled by instantaneous changes to the functional form of the vector field describing the evolution of the dynamic system at points in time known as *events*. Typically, the time of occurrence of such events is marked by the system state satisfying some condition, such as the familiar pressure ratio threshold defining the transition from choked to unchoked flow, or vice versa. Hence, these events are implicit in the sense that their time of occurrence is not known in advance, but must be determined from the evolution of the system state.

The study of such discontinuous dynamic systems has attracted increasing attention in recent years, and the terminology hybrid (discrete/continuous) systems has become popular. Given the many applications of hybrid system representations, it is natural to consider the next step and develop the theory and numerics necessary for systematic optimization of hybrid dynamic systems. In fact, classical optimality conditions for a quite general class of ODE embedded hybrid systems are stated in at least one standard text [1][pp. 106–108]: given a known sequence of events, at each of which both the functional form of the vector field and the state may be discontinuous, Euler-Lagrange necessary conditions may be derived. Moreover, this derivation highlights two separate and distinct features of the optimal control thus defined: a) the sequence of events that characterizes the optimal trajectory, especially those of the implicit character mentioned above, and b) the optimal control profiles corresponding to this sequence. Clearly many practical problems may be characterized by several alternative sequences of events, and it would be desirable to search over these alternatives to find the optimal sequence. Or, in other words, hybrid optimal control has the potential to make simultaneously control profile and sequencing decisions in the optimization of a dynamic system. Unfortunately, to our knowledge, the classical analysis provides no further guidance on how to conduct this search over alternative sequences of events; if the sequence is known, the optimal control profiles may be found, but how can the optimal sequence be found without a combinatorial enumeration of sequences? This paper presents our preliminary progress towards this goal.

MODEL AND OPTIMIZATION FORMULATION

We consider a broad class of DAE embedded hybrid systems described by a state space $S = \bigcup_{k=1}^{n_k} S_k$ where each *mode* S_k is characterized by:

1. A set of variables $\{\dot{\mathbf{x}}^{(k)}, \mathbf{x}^{(k)}, \mathbf{y}^{(k)}, \mathbf{u}^{(k)}, \mathbf{p}, t\}$, where $\mathbf{x}^{(k)} \in \mathbf{R}^{n_x^{(k)}}$ are the differential state variables, $\mathbf{y}^{(k)} \in \mathbf{R}^{n_y^{(k)}}$ the algebraic state variables and $\mathbf{u}^{(k)} \in \mathbf{R}^{n_u^{(k)}}$ the controls. The time invariant parameters $\mathbf{p} \in \mathbf{R}^{n_p}$ and time t are independent variables.
2. A set of equations:
$$\mathbf{f}^{(k)}(\dot{\mathbf{x}}^{(k)}, \mathbf{x}^{(k)}, \mathbf{y}^{(k)}, \mathbf{u}^{(k)}, \mathbf{p}, t) = \mathbf{0} \tag{1}$$
where $\mathbf{f}^{(k)} : \mathbf{R}^{n_x^{(k)}} \times \mathbf{R}^{n_x^{(k)}} \times \mathbf{R}^{n_y^{(k)}} \times \mathbf{R}^{n_u^{(k)}} \times \mathbf{R}^{n_p} \times \mathbf{R} \rightarrow \mathbf{R}^{n_x^{(k)}+n_y^{(k)}}$. It is assumed that in mode S_k, specification of the parameters $\mathbf{p}$ and the controls $\mathbf{u}^{(k)}$ coupled with a consistent initial condition $\mathbf{T}_k(\dot{\mathbf{x}}^{(k)}, \mathbf{x}^{(k)}, \mathbf{y}^{(k)}, \mathbf{u}^{(k)}, \mathbf{p}, t) = \mathbf{0}$ at $t = t_0^{(k)}$ determines a unique solution in $[t_0^{(k)}, t_f^{(k)})$.
3. A (possibly empty) set of transitions to other modes. The set of modes S_j where a transition from mode S_k is possible is $J^{(k)}$. The transitions are described by:
   (a) Transition conditions:
$$L_j^{(k)}(\dot{\mathbf{x}}^{(k)}, \mathbf{x}^{(k)}, \mathbf{y}^{(k)}, \mathbf{u}^{(k)}, \mathbf{p}, t) \quad j \in J^{(k)} \tag{2}$$
   determining the transition times (or events) $t = t_f^{(k)}$ at which switching from mode k to mode j occurs. The transition conditions are formed by logical propositions that trigger the switching when they become true, and consist of logical operators ($\neg$, $\wedge$, $\vee$) connecting atomic propositions (relational expressions) composed of valid real expressions and the relational operators $\{>, <, \leq, \geq\}$. Associated with every relational expression we can consider a discontinuity function:
$$g_{ji}^{(k)}(\dot{\mathbf{x}}^{(k)}, \mathbf{x}^{(k)}, \mathbf{y}^{(k)}, \mathbf{u}^{(k)}, \mathbf{p}, t) \quad i = 1, \ldots, n_j^{(k)} \tag{3}$$

formed by the difference between the two real expressions. Each relational expression changes its value whenever its corresponding discontinuity function crosses zero. A more detailed discussion can be found in [3]. Note that discontinuities in the controls are included here.

(b) Transition functions:

$$\mathbf{T}_j^{(k)}(\dot{\mathbf{x}}^{(k)}, \mathbf{x}^{(k)}, \mathbf{y}^{(k)}, \mathbf{u}^{(k)}, \dot{\mathbf{x}}^{(j)}, \mathbf{x}^{(j)}, \mathbf{y}^{(j)}, \mathbf{u}^{(j)}, \mathbf{p}, t) \quad j \in J^{(k)} \tag{4}$$

are associated with the transition conditions, relating the variables in the mode S_k and the variables in the new mode S_j at the transition time $t = t_f^{(k)}$. A special case of the transition functions is the set of initial conditions for the initial mode S_1. This will be designated by $\mathbf{T}_1^{(0)}$.

Note that integer variables can be represented in this formulation by using a different mode for every value of the variable. Two classes of constraints may be imposed on such hybrid dynamic systems:

1. Path constraints. These must be satisfied along the entire trajectory in a particular mode:

   (a) Inequality path constraints:

$$\mathbf{h}^{(k)}(\dot{\mathbf{x}}^{(k)}, \mathbf{x}^{(k)}, \mathbf{y}^{(k)}, \mathbf{u}^{(k)}, \mathbf{p}, t) \leq \mathbf{0} \tag{5}$$

   (b) Equality constraints. These can be treated as addition equations of the DAE [4], effectively reducing the number of independent controls in that mode.

   Note that the path constraints enforced may be completely different from one mode to the next, so that certain path constraints may only hold over subintervals of the overall time interval.

2. Point constraints. These must be satisfied only at specific times:

   (a) Inequality constraints:

$$\mathbf{c}_r^{(k)}(\dot{\mathbf{x}}^{(k)}, \mathbf{x}^{(k)}, \mathbf{y}^{(k)}, \mathbf{u}^{(k)}, \mathbf{p}, t_r) \leq \mathbf{0} \quad r \in \{0, ..., n_r^{(k)}\} \tag{6}$$

   (b) Equality constraints. The initial and final conditions are point constraints:

$$\mathbf{c}_s^{(k)}(\dot{\mathbf{x}}^{(k)}, \mathbf{x}^{(k)}, \mathbf{y}^{(k)}, \mathbf{u}^{(k)}, \mathbf{p}, t_s) = \mathbf{0} \quad s \in \{0, ..., n_s^{(k)}\} \tag{7}$$

   Again, the point constraints enforced may differ from one mode to the next.

The compact expression of an objective function is complicated by the possibility of different sets of variables characterizing each mode, and the fact that the optimal sequence of mode transitions, and thus the active mode at the final time, are not known a priori. One solution to these complications is to define a dummy zero duration terminal mode labeled $n_k + 1$, and require a terminal transition (i.e., with transition function) from every other mode to this terminal mode at the final time for the overall problem, denoted t_f. This construct allows the formulation of a Mayer type objective function:

$$\min_{\mathbf{u}(t), \mathbf{p}, t_f} \phi(\dot{\mathbf{x}}^{(n_k+1)}(t_f), \mathbf{x}^{(n_k+1)}(t_f), \mathbf{y}^{(n_k+1)}(t_f), \mathbf{p}, t_f) \tag{8}$$

Clearly, this can be made equivalent to Lagrange or Bolza type objective functions through the introduction of additional state variables. Further, terms related to the cost of transitions can be incorporated by introducing state variables whose values are modified by the transition functions.

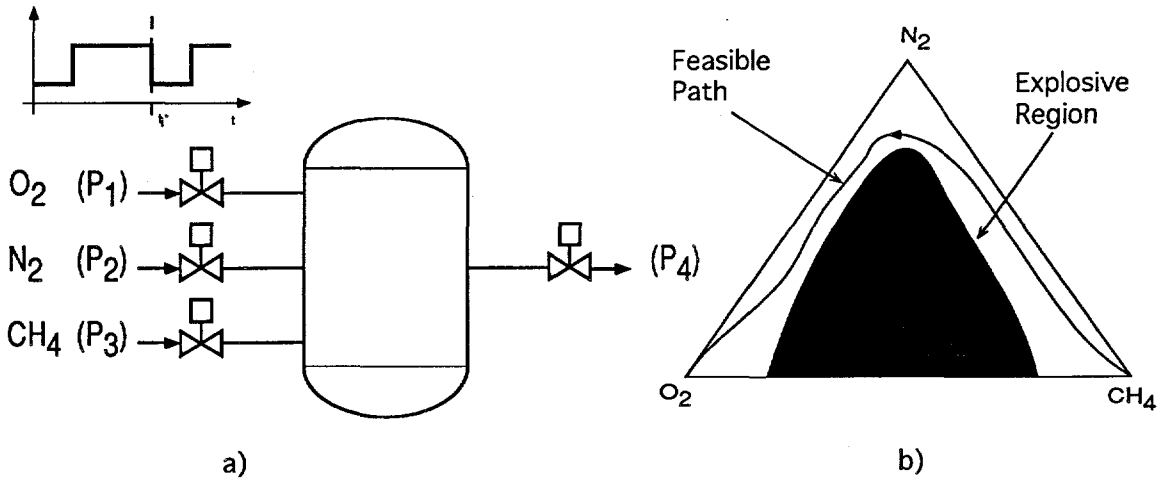

Figure 1: Tank Changeover Problem: a) process flowsheet. b) composition space

TANK CHANGEOVER EXAMPLE

As an example, consider the design of a changeover operation for a vessel in a chemical process (Figure 1). We wish to move safely in minimum time from an initial state in which methane is flowing through the system to a final state in which oxygen is flowing, taking into account important quantitative features of the problem. The purpose of this example is to demonstrate that given a hybrid dynamic model, and the point and path constraints representing safety and operational goals/constraints, a hybrid dynamic optimization procedure can in principle design the changeover policy automatically. In order to present a relatively compact model, we assume isothermal conditions:

$$\left.\begin{array}{l} \dot{M}_j = N_1 y_{1j} + N_2 y_{2j} + N_3 y_{3j} - N_4 y_{4j} \\ M_j = M_T y_j \\ y_{4j} = y_j \end{array}\right\} \forall j \in J \tag{9}$$

$$\sum_{j \in J} y_j = 1 \qquad PV = M_T RT \tag{10}$$

$$N_i = \left\{ \begin{array}{ll} 0 & \text{if } \frac{P}{P_i} \geq 1 \\ u_i C_v A_i \sqrt{\frac{P_i + P}{2}} \frac{P_i - P}{b + \sqrt{P_i - P}} & \text{if } 0.53 < \frac{P}{P_i} < 1 \\ u_i C_v A_i \frac{P_i}{\sqrt{2}} 0.85 & \text{if } \frac{P}{P_i} \leq 0.53 \end{array} \right\} \quad \forall i = 1 \ldots 3 \tag{11}$$

$$N_4 = \left\{ \begin{array}{ll} 0 & \text{if } \frac{P_4}{P} \geq 1 \\ u_4 C_v A_4 \sqrt{\frac{P_4 + P}{2}} \frac{P - P_4}{b + \sqrt{P - P_4}} & \text{if } 0.53 < \frac{P_4}{P} < 1 \\ u_4 C_v A_4 \frac{P}{\sqrt{2}} 0.85 & \text{if } \frac{P_4}{P} \leq 0.53 \end{array} \right. \tag{12}$$

where $I = \{1, 2, 3, 4\}$ is an index set for the valves, $J = \{O_2, N_2, CH_4\}$ is an index set for the chemical species present, P_1, P_2, P_3 are the known supply pressures of O_2, N_2 and CH_4 respectively, P_4 is the known discharge pressure, V is the fixed volume of the system determining the holdup, and the mole fractions $y_{i=1\ldots3, j \in J}$ are given by the composition of the corresponding pure species. The controls $u_{i \in I}(t) \in \{0, 1\}$ are the time profiles of the on/off signals to the four open/close valves.

Equations (11–12) model the gas flow through valves, distinguishing between laminar/turbulent and choked regimes. The model itself also enforces the path constraint of no reverse flow through

the valves. Although this requirement could be enforced equivalently through the introduction of inequality path constraints, the latter formulation would require further modes in the model that adjust the intensive properties (i.e., composition) of the flow through each valve with the direction of flow. This latter option is particularly undesirable because it introduces the complication of defining the composition of the outlet flow when $P_4 > P$. Note that, since at any point in time each valve may independently be in any one of its three modes, the overall system has 3^4 modes. However, most of the model equations are common to all modes (equations (9–10)), so notation such as that used above is more convenient than explicitly enumerating all the modes [5]. All transition functions apart from the initial condition enforce continuity of $M_{j\in J}$.

The point and path constraints define the changeover policy required. In this example we have point constraints defining the initial condition and final target composition:

$$y_{O_2}(0) = 0 \quad y_{CH_4}(0) = 1 \quad P(0) = P_0 \tag{13}$$

$$y_{O_2}(t_f) \geq 0.999 \tag{14}$$

Clearly, the initial mode is chosen to be consistent with the initial pressure, although in general it may have to be specified explicitly. The key safety consideration is to avoid the formation of an explosive mixture in the vessel at any time during the changeover. If a curve bounding the explosive region of $O_2/N_2/CH_4$ mixtures in composition space is constructed, this curve can be used to formulate an inequality path constraint:

$$h(y_{O_2}(t), y_{CH_4}(t)) \leq 0 \tag{15}$$

that must hold in every mode. Interestingly, this approach implicitly infers the need for a N_2 purge before introducing O_2 from the existence of the path constraint in the formulation. Other path constraints, such as the equipment limits (e.g., design pressure), are also easily incorporated.

ANALYSIS

A particular operating procedure in the above example is defined by the control profiles $u_{i\in I}(t)$, which specify the sequence of openings/closings of the four valves along a particular transient. Since these are open/close valves, the signals are binary variables, and the problem as stated above might be termed a mixed-integer optimal control problem; i.e., optimal control profiles over time for a set of binary variables are required. This factor further complicates the variational analysis of such problems, which (as yet) is already confounded by the absence of results that guide determination of the sequence of mode transitions that characterizes the optimal trajectory (see above).

These complications with the variational analysis have prompted us to study a related class of problems, namely parameter optimization of hybrid dynamic systems. In this class of problems the set of decision variables is reduced to the time invariant parameters $\mathbf{p}$, and hence the problem becomes a finite dimensional optimization problem with a hybrid dynamic system embedded, rather than an infinite dimensional optimal control problem. Our efforts have two major motivations: a) parameter optimization of hybrid dynamic systems is an important and interesting class of problems in its own right, and in addition this study may yield useful insights for the more complex infinite dimensional problems, and b) the most widely used methods for numerical optimal control of complex large-scale problems rely on approximation of the infinite dimensional problem by a finite dimensional parameter optimization problem, either via discretization of the controls or discretization of both controls and states [6].

For example, *control parameterization* [2] approximates the controls with a finite set of basis functions (e.g., Lagrange polynomials on finite elements), and thus the controls in the above formulation become dependent variables $\mathbf{u}^{(k)}(\mathbf{p}, t)$. For numerical solution of the resulting parameter optimization problem, this discretization yields a decomposition into two subproblems: a) an IVP subproblem in which the hybrid system model is solved for given values of $\mathbf{p}$ using combined discrete/continuous simulation technology [5, 3], and b) an NLP Master problem that searches in the finite parameter space using function and constraint information furnished by the IVP subproblem. If the Master NLP is to be solved using an efficient gradient-based search, gradient information must be extracted in some manner from the embedded dynamic system. Although there are a number of ways of doing this, probably the most efficient method at present is to solve the dynamic system and its related sensitivity systems simultaneously to determine the parametric sensitivities [7], and then apply the chain rule to these sensitivities to extract gradients.

While existence and uniqueness results for the parametric sensitivities of a continuous dynamic system are well known [8], the existence of parametric sensitivities of a (discontinuous) hybrid system, and hence the feasibility of the above procedure, was an open question. In [9] we prove sufficient conditions for the existence and uniqueness of the parametric sensitivities for the class of hybrid systems outlined above. These results are particularly illuminating because they suggest that, perhaps surprisingly, in general the sensitivities of a hybrid system exist almost everywhere in parameter space. Further, this observation yields a preliminary classification for hybrid parameter optimization problems. Roughly speaking, if the sequence of implicit mode transitions along the transient is the same at every point in parameter space, the sufficient conditions hold, the sensitivities are guaranteed to exist everywhere and can be calculated numerically, and a smooth Master NLP results. Thus, our results make possible for the first time solution of this class of hybrid parameter optimization problems with efficient gradient based procedures. On the other hand, if the sequence of implicit mode transitions can differ from region to region of parameter space (i.e., the optimization is searching over a number of alternative sequences of events, our original goal), our sufficient conditions are no longer guaranteed to hold, particularly at those points in parameter space where the sequence changes qualitatively. Although we are still studying the properties of the sensitivity trajectories when our conditions do not hold, numerical experience indicates that often such points in parameter space correspond to points of nondifferentiability or discontinuity in the Master NLP. Thus, we conclude that numerical parameter optimization of hybrid dynamic systems encompassing automated sequencing decisions may indeed be possible, provided at least the optimization procedure employed can deal with nondifferentiability and/or discontinuity in the Master NLP.

RESULTS AND DISCUSSION

So, is the inherent nonsmoothness of the Master NLP the only complication in the use of a control parameterization approach to make sequencing decisions in a hybrid dynamic system? In order to test this hypothesis, we solved the tank changeover example using a direct stochastic search procedure that is relatively insensitive to nonsmoothness and/or multi-modality of the Master NLP. The particular procedure used was a modification of the ICRS algorithm [10]. Objective function and constraint evaluations were furnished by calls to the ABACUSS process simulator, which was required to solve the hybrid IVP subproblem with extremely high reliability. Some preliminary results corresponding to a changeover time of 238.68s are shown in Figure 2. These results are a promising indication that nonsmoothness may be the only complication in many problems of practical relevance.

The results presented in Figure 2 were generated using a control parameterization that obviates

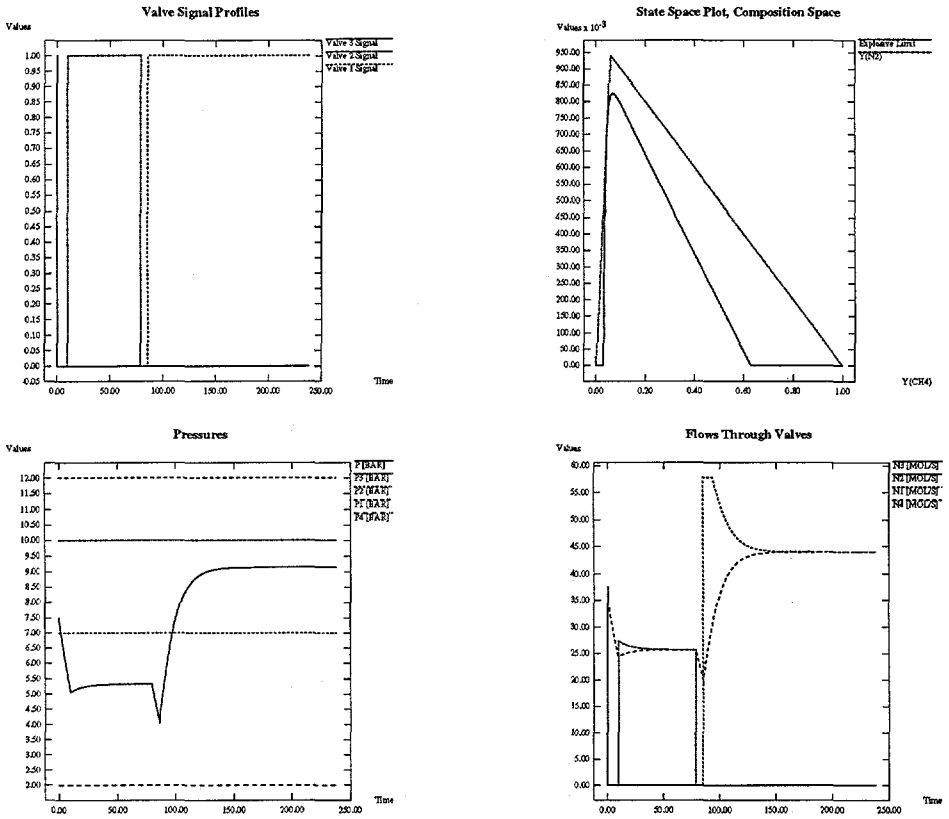

Figure 2: Tank Changeover Problem. Preliminary Results.

the need for binary decision variables. Since the initial valve signal values are known, one possible control parameterization is to allow the control signals to flip value ($0 \rightarrow 1$ or $1 \rightarrow 0$) at a finite number of points in time. Thus, the decision variables in the parameter optimization problem become these transition times, a set of continuous variables. Provided the optimal solution does not involve an infinite number of such transitions, introducing a sufficient number of transitions in the control parameterization should embed the true optimal control within the search space.

However, this control parameterization does not eliminate the nonsmooth character of the problem. In addition to a series of transition times for the valve signals, the optimization procedure has determined the sequence of flow transitions in each of the valves along the optimal trajectory. In particular, a study of the flow profiles plot indicates that a transition from choked to unchoked flow occurs in valve 1 soon after it is opened. Similarly, the procedure has determined the sequence of activations and deactivations of the inequality path constraint along the optimal trajectory (see the composition state space plot). Several numerical procedures for the numerical treatment of inequality path constraints (including the penalty approach employed in this particular case) effectively formulate an equivalent hybrid dynamic optimization, and solve this problem [2, 11]. Although computationally expensive, the stochastic search procedure appears to be able to find reasonable solutions in the presence of nonsmoothness and multi-modality.

CONCLUSIONS

These preliminary results show that a nonsmooth approach to parameter optimization of hybrid

dynamic systems is potentially a very promising approach to the automation of sequencing decision in dynamic systems. However, much work remains. At present, due to the heuristic termination criteria of the stochastic search procedure, we are not even sure the solutions presented above are locally optimal. Assuming Lipschitz continuity of the Master NLP, Kuhn-Tucker type optimality conditions for nonconvex nonsmooth problems are known [12], but it still remains to be determined how the information required to test for local optimality (e.g., directional derivatives) can be propagated through a hybrid dynamic system.

Similarly, more efficient numerical solution of the resulting nonsmooth Master NLPs is an open issue. Bearing in mind the existence of sensitivity information, and our understanding of the origin of the nonsmoothness, the development of at least efficient local search methods seems a distinct possibility. On the other hand, if the sequence of mode transitions is fixed a priori [4], efficient gradient based search for the optimal profiles for a given sequence is now possible. However, given this smooth subproblem, a combinatorial search over many alternative sequences would be required as a Master problem, and generic solution procedures for such mixed-integer dynamic optimization problems suffer from the property of unpredictable convergence to arbitrary suboptimal points [13]. Thus, the nonsmooth approach appears at present to be more promising.

Acknowledgements — This work was supported by the United States Department of Energy under grant DE-FG02-94ER14447.

REFERENCES

[1] A. E. Bryson and Y. Ho. *Applied Optimal Control.* Hemisphere, New York, 1975.

[2] K. Teo, G. Goh, and K. Wong. *A Unified Computational Approach to Optimal Control Problems.* Pitman Monographs and Surveys in Pure and Applied Mathematics. Wiley, New York, 1991.

[3] T. Park and P. I. Barton. State event location in differential-algebraic models. *ACM Trans. Mod. Comput. Sim.*, 6(2):137–165, 1996.

[4] W. F. Feehery. *Dynamic Optimization with Path Constraints.* PhD thesis, Massachusetts Institute of Technology, 1998.

[5] P. I. Barton. *The Modelling and Simulation of Combined Discrete/Continuous Processes.* PhD thesis, University of London, 1992.

[6] D. Kraft. On converting optimal control problems into nonlinear programming problems. *Comp. Math. Prog.*, 15:261–280, 1985.

[7] W. F. Feehery, J. E. Tolsma, and P. I. Barton. Efficient sensitivity analysis of large-scale differential-algebraic systems. *Appl. Num. Math.*, 25(1):41–54, 1997.

[8] T. H. Gronwall. Note on the derivatives with respect to a parameter of the solutions of a system of differential equations. *Annals of Mathematics*, 20:292–296, 1919.

[9] S. Galán, W. F. Feehery, and P. I. Barton. Parametric sensitivity functions for hybrid discrete/continuous systems. *Appl. Num. Math.*, 1998. submitted.

[10] J. R. Banga and J. J. Casares. Integrated controlled random search: Application to a wastewater treatment plant model. *IChemE Symposium Series*, 100:183–192, 1987.

[11] W. F. Feehery and P. I. Barton. Dynamic optimization with state variable path constraints. *Computers chem. Engng*, 22(6), 1998. in press.

[12] K. Shimizu, Y. Ishizuka, and J. F. Bard. *Nondifferentiable and Two-Level Mathematical Programming.* Kluwer, Boston, 1997.

[13] R. J. Allgor and P. I. Barton. Mixed integer dynamic optimization. *Computers chem. Engng*, 21(S):S451–S456, 1997.

"STABILITY AND SAFE OPERATION FOR LOW-DENSITY POLYETHYLENE REACTORS"

Carlos M. Villa, Z. Gene Xu, and W. Harmon Ray

Department of Chemical Engineering
University of Wisconsin
Madison, WI 53706

ABSTRACT

The problems of reactor stability and explosive runaway in low-density polyethylene autoclaves are addressed. The effects of imperfect mixing on the macro-and microscale are analyzed with surprising results. It is found that imperfect macromixing greatly improves the reactor stability characteristics and reduces the possibility of explosive ethylene decomposition episodes. The analysis methods allow one to tune the initiator mix to provide both increased conversion and robust stability. Finally, the phenomenon of reactor hot spots is discussed with analysis by computational fluid mechanics.

INTRODUCTION

Low-density polyethylene (LDPE) is one of the largest volume polymers produced in the world. It is produced in both autoclave and tubular reactors. One autoclave process, shown in Figure 1, is indicative of the operating conditions used. The reactor operates adiabatically at relatively high temperatures and at extremely high pressures. Because of the high rate of reaction under these conditions, the reactor residence times must be kept very short to limit the temperature rise in the reactor. The adiabatic temperature rise for complete conversion of ethylene to polymer is ~1300°C; thus the monomer conversion is kept in the range of 10-20%.

The reactor temperature may be regulated to some degree by controlling the feedrate of free-radical producing initiator. Unfortunately, there are also highly exothermic ethylene decomposition reactions that become significant above about 310°C as illustrated in Figure 2. These reactions require only ethylene as a reactant and have an overall adiabatic temperature rise of ~2000°C. Thus once decomposition begins, it cannot be stopped and measures must be taken to vent the contents of the reactor before the reactor explodes.

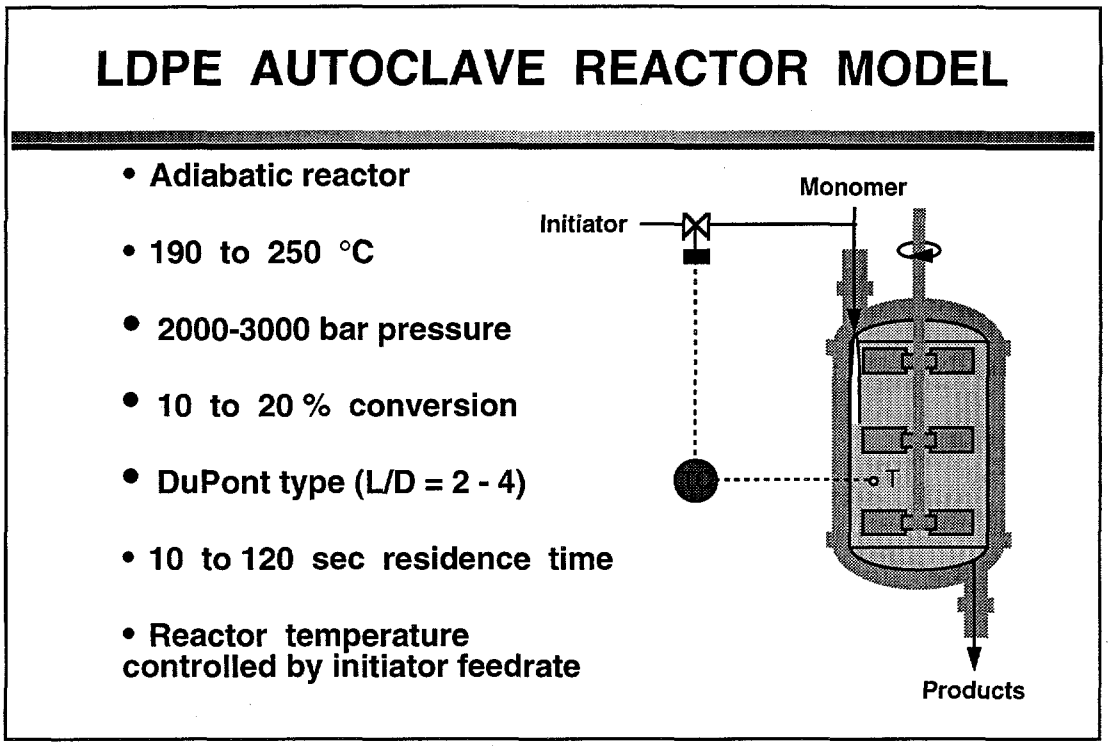

Figure 1 The LDPE Autoclave Reactor

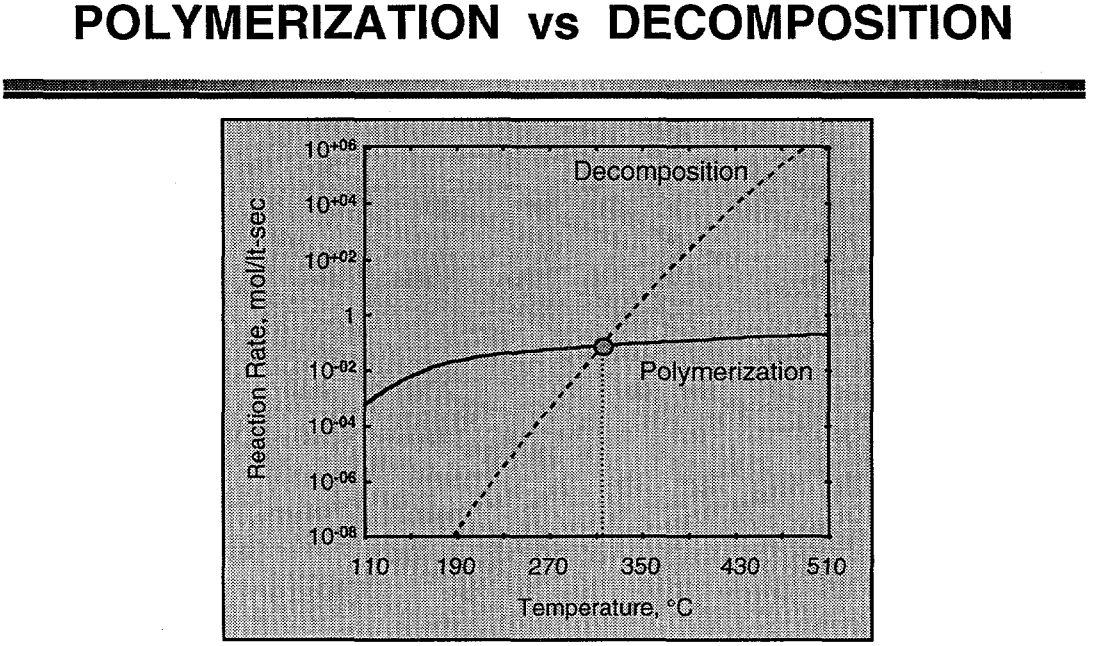

Figure 2 The relative rates of polymerization and ethylene decomposition

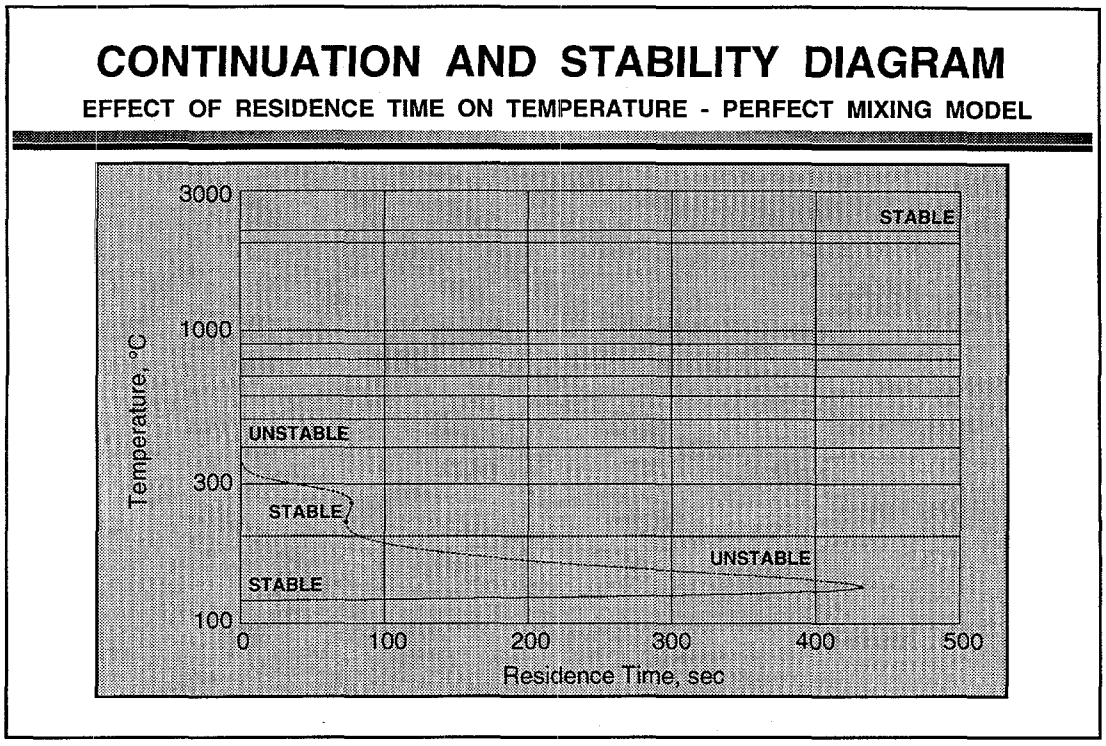

Figure 3 The bifurcation diagram for perfect mixing

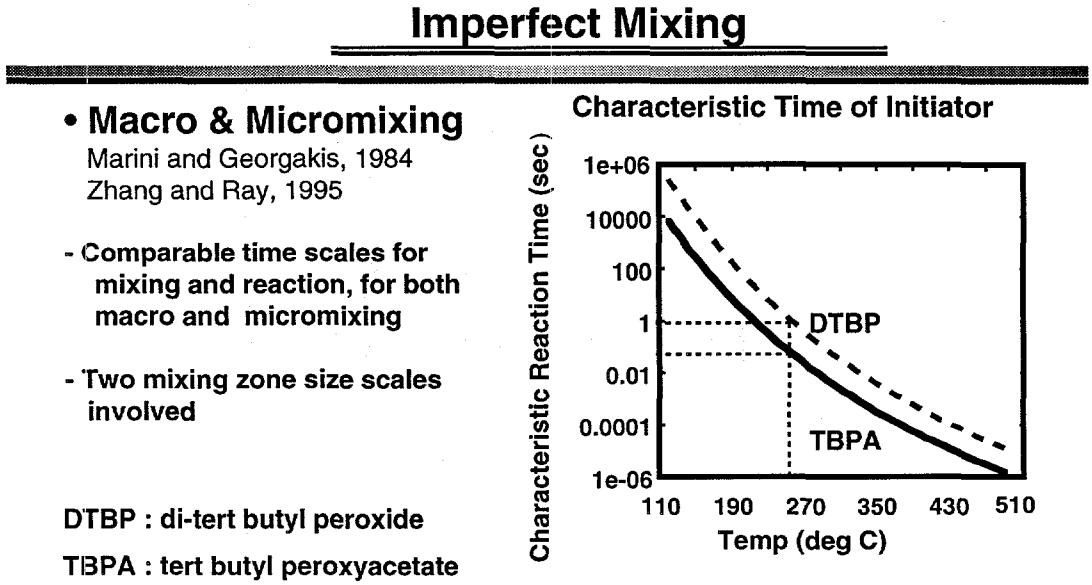

Figure 4 The reasons for imperfect mixing

REACTOR BEHAVIOR

Zhang et.al. [1] have modeled both the polymerization and decomposition reactions and determined the bifurcation behavior of the reactor assuming the autoclave is well mixed. Figure 3 shows the stability structure under these conditions. Note that the desired operating temperature of ~250°C is stable, but the curve is so steep that there is poor robustness to disturbances. Thus even with a good control system, one could very easily drop to the lower stable steady state where the reaction ceases, or be carried away towards a ~2000°C upper steady state.

As shown in Figure 4, the characteristic reaction times for the commonly used initiators are ~0.1-1 sec. at reactor conditions. This means that the reactor is not perfectly mixed at either the macro or microscale. First, we will look at the effects of imperfect macroscale mixing and then discuss microscale mixing issues. Many groups have used computational fluid mechanics (CFD) methods to simulate detailed velocity, concentration, and temperature fields in polymer reactors. In our first work [2], we were able to simulate some of the effects of imperfect mixing on a similar reactor. However, these computations can be limited by computer speed and problem size at the moment.

Recognizing that mixing of the feed plume is the most serious macromixing issue in LDPE reactors, a study using a compartment model was carried out [3]. As shown in Figure 5, two small stirred tanks were used to represent the feed plume, and the recirculating flows (streams 4 and 5 on the figure) are adjusted to match experimental initiator consumption and residence time distribution data. The bifurcation diagram for this imperfectly mixed reactor, (cf. Figure 6) is very similar to the perfectly mixed reactor when the circulation rates, R, are large. However, for intermediate values (R = 10-20) where the experimental initiator consumption data are well represented by the model, note the dramatic increase in size of the stable middle branch. With imperfect macromixing the reactor is very robust to fluctuations in residence time. This robustness extends to all other disturbances which could cause temperature upsets, as illustrated for feed initiator concentration in Figure 7.

These compartment models are very useful for tuning the mixture of initiators commonly used with these reactors. Figure 8 shows that a relatively low temperature initiator gives very robust reactor behavior. However, a high temperature initiator, which may be used to increase conversion slightly, may destabilize the reactor. However, a proper mixture (curve M) may give acceptable robustness and higher conversion.

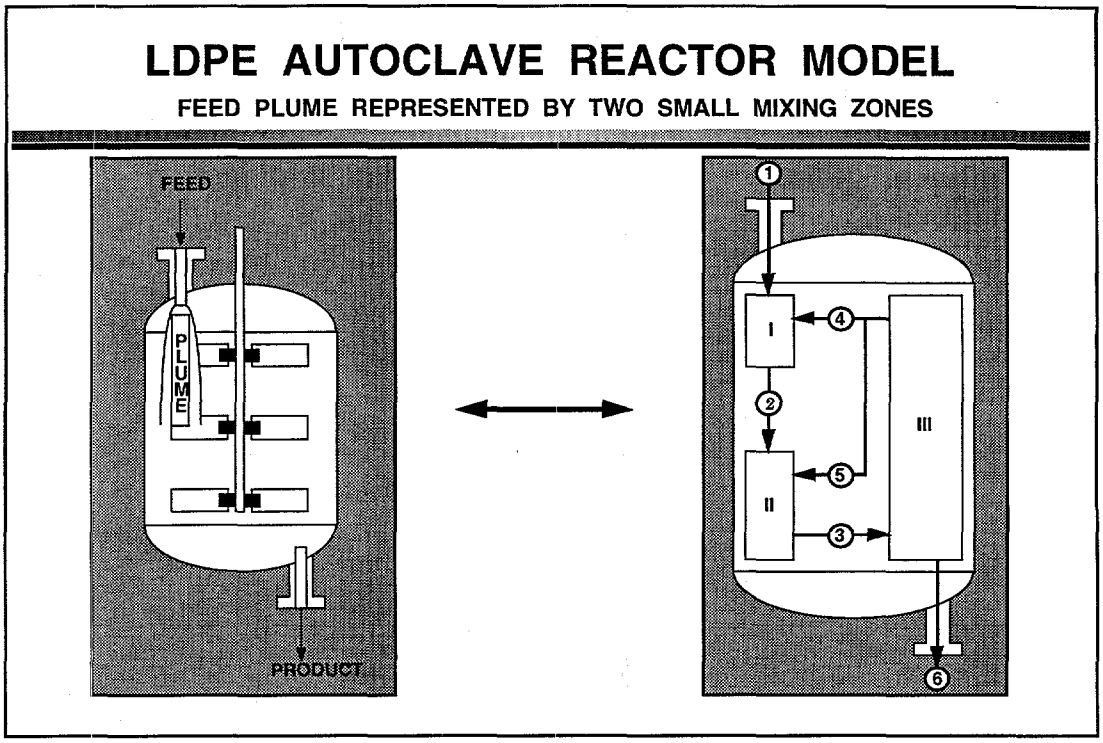

Figure 5 A compartment model for imperfect macromixing of the feed material

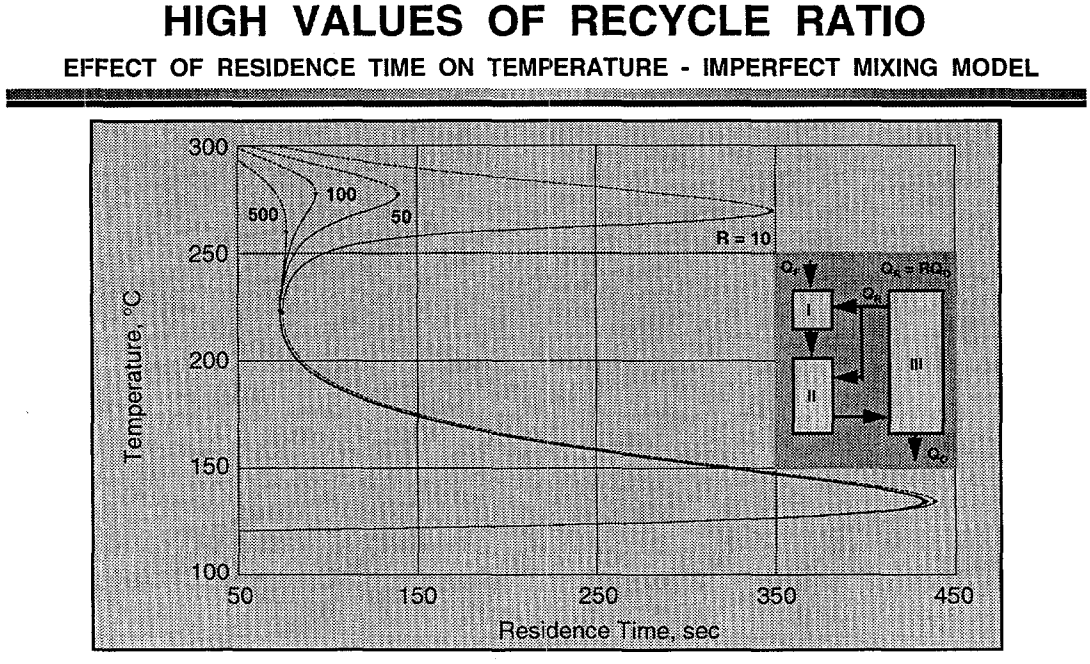

Figure 6 Bifurcation diagrams for various levels of imperfect macromixing

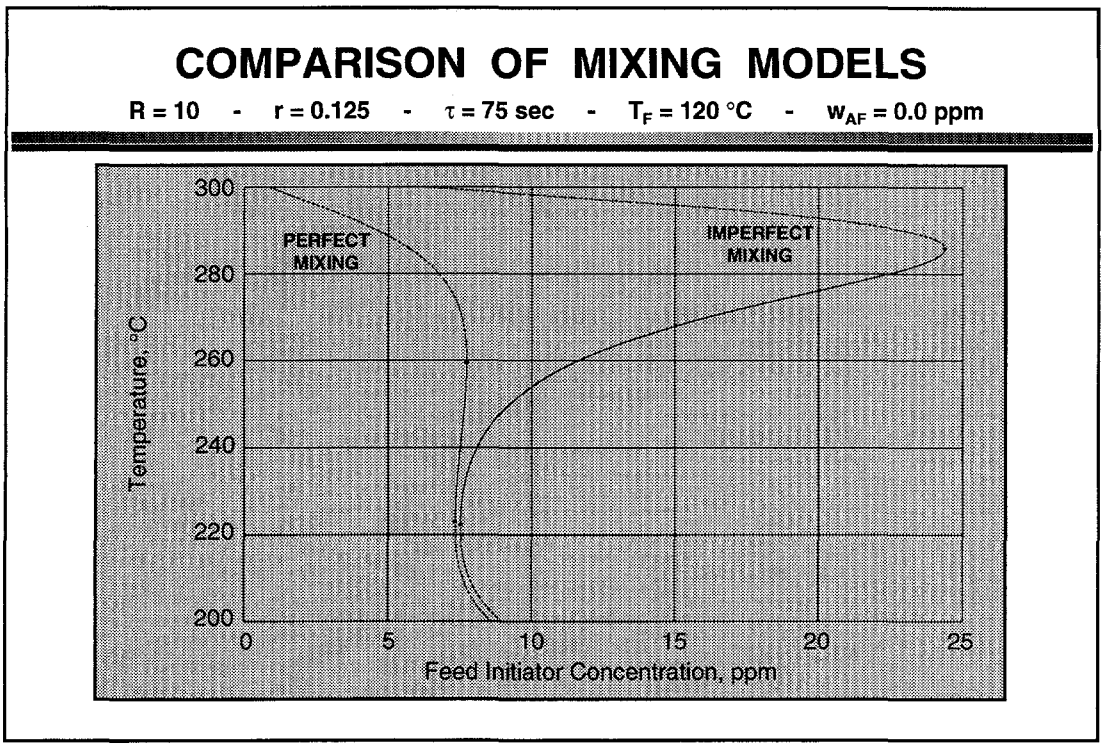

Figure 7 Comparison of bifurcation diagrams for initiator feed concentration

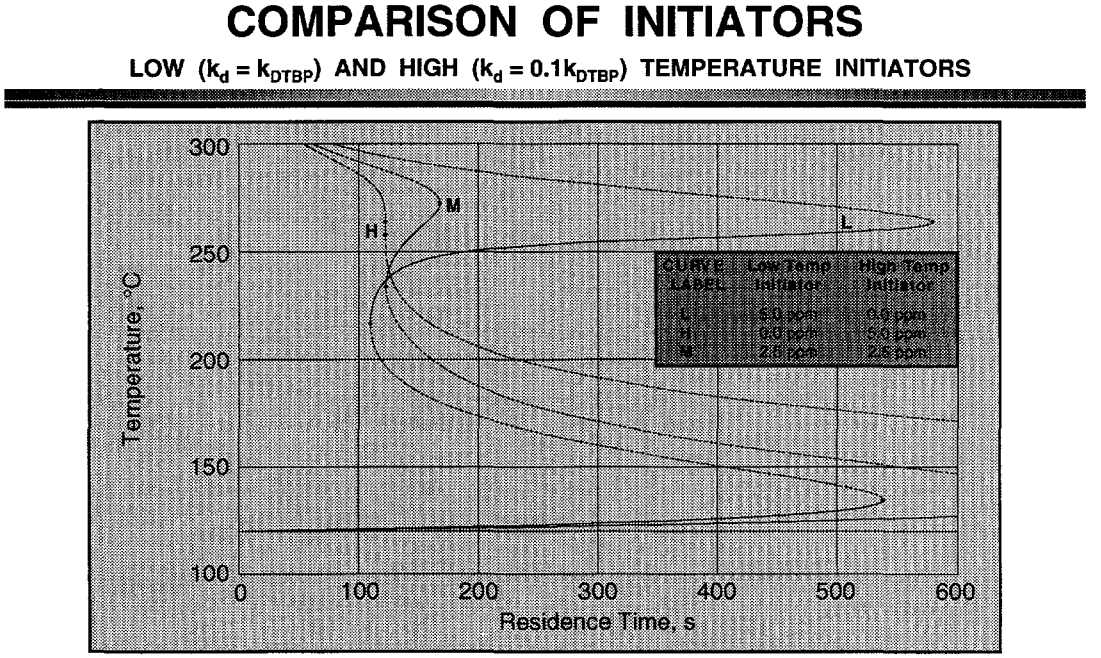

Figure 8 Bifurcation diagrams for various initiator cocktails

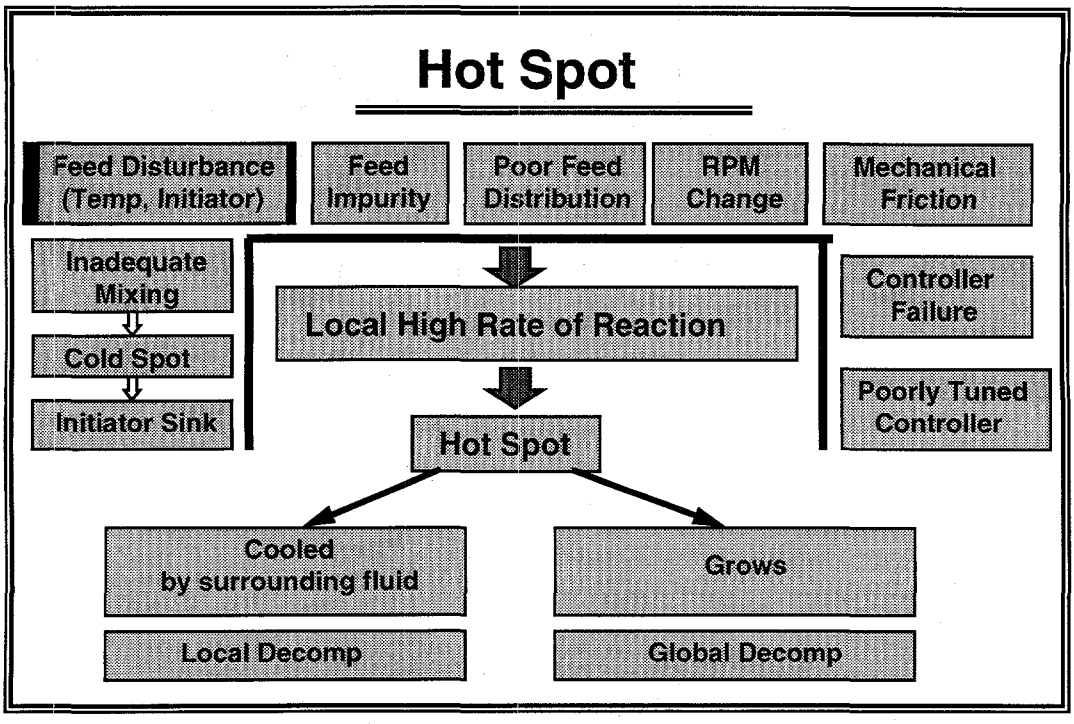

Figure 9 Hot spot phenomena – possible causes and outcomes

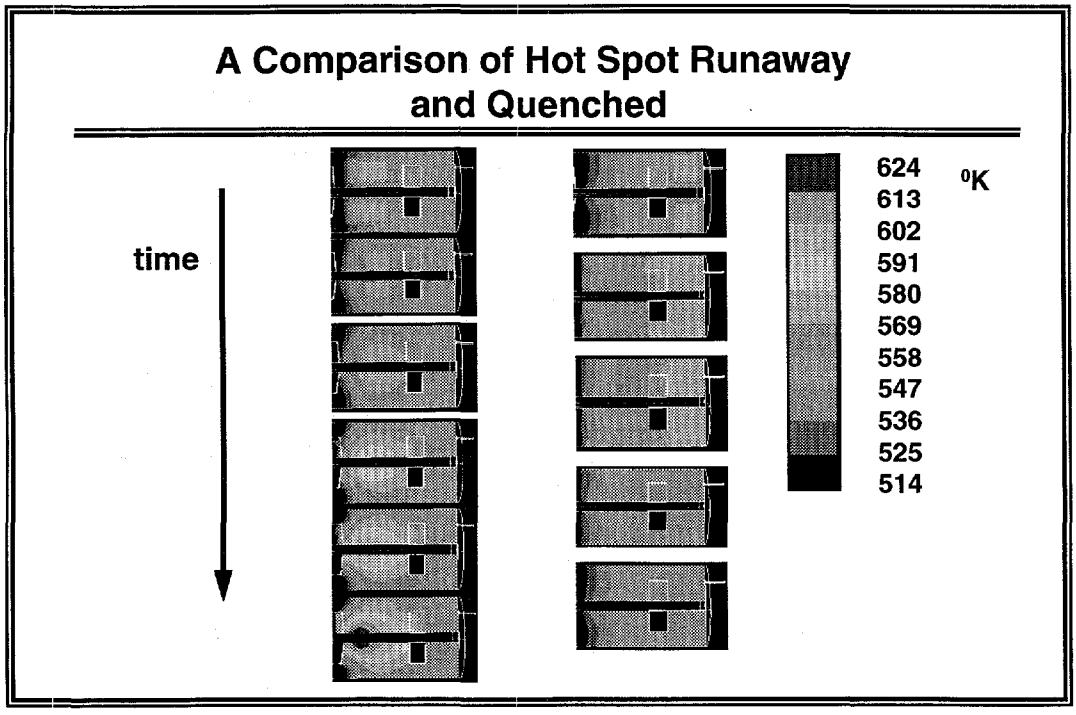

Figure 10 Illustration of hot spot outcomes; left: hot spot causes global runaway; right: hot spot is quenched

A second class of phenomena which can arise due to imperfect mixing is the occurrence of hot spots in the reactor. As indicated in Figure 9, there can be a variety of causes of these hot spots. Once they arise, there are two possible outcomes: (i) the hot spot can be quenched by surrounding fluid and disappear or, (ii) the hot spot can grow and eventually cause a global decomposition in the reactor. Hot spot scenarios – both cause and effect – are being studied in our group [4]. Figure 10 illustrates the two possible outcomes for a large scale hot spot in the bottom and in the top of the reactor.

CONCLUSION

Through a detailed reactor model, including both polymerization and ethylene decomposition reactions, the dynamic behavior of low-density polyethylene autoclave reactors has been analyzed. Using CFD methods and compartment models, the effects of imperfect macro- and microscale mixing can be predicted. One remarkable result is that imperfect macroscale mixing greatly improves the stability characteristics of the reactor. Hot spot phenomena have also been studied to determine whether they are quenched or lead to global reactor runaway. This research is continuing.

ACKNOWLEDGEMENT

This work was performed under the auspices of the U. S. Department of Energy.

REFERENCES

1. Zhang, Simon X., Nolan K. Read, and W. H. Ray. "Runaway Phenomena in Low Density Polyethylene Autoclave Reactors". *AIChE Journal* 42, 10, .2911-2924 (1996).

2. Read, N. K., S. X. Zhang, and W. H. Ray. "Simulations of a LDPE Reactor Using Computational Fluid Dynamics". *AIChE Journal*, 43, 1, 104-117 (1997).

3. Villa, C. M., J. O. Dihora and W. H. Ray. "Effects of Imperfect Mixing on LDPE Reactor Dynamics". *AIChE Journal* (in press).

4. Xu, Z. Gene and W. Harmon Ray. "Ethylene Decomposition and Hot Spot Phenomena in Low-Density Polyethylene Autoclave Reactors", Manuscript to be submitted to *AICHE Journal*.

Optimization Strategies for the Synthesis and Operation of Chemical Process Systems

I.E. Grossmann, L.T. Biegler and A.W. Westerberg
Department of Chemical Engineering
Carnegie Mellon University
Pittsburgh, PA 15213

ABSTRACT

This paper reviews three projects by our group at Carnegie Mellon, all of which have in common that they give rise to multiperiod design and operation optimization problems. The first project deals with the synthesis and operation of multiperiod energy systems in which effective decomposition algorithms have been proposed for solving large multiperiod mixed-integer programming problems. The second project deals with simultaneous design, scheduling and dynamic operation of batch processes in which effective models are proposed to integrate the multiple objectives. The third project deals with the synthesis of flexible distillation sequences in which a hybrid solution approach is proposed that relies on the use of branch and bound, and cooperative algorithms that use simulated annealing and genetic algorithms.

INTRODUCTION

One of the recent trends in process systems engineering has been to anticipate operational issues at the design stage. In this paper we illustrate in three different areas of applications how these issues can be incorporated in design models. The first part will illustrate the use of multiperiod optimization models for operation of utility plants, and that can be extended to design problems using mixed-integer programming as the basic framework. The second part will illustrate the integration of operational dynamic models with aggregated scheduling models for multiproduct batch processes. Finally, the third part will illustrate the application of insights and hybrid methods for the design of flexible distillation sequences.

STRATEGIES FOR THE SYNTHESIS AND OPERATION OF MULTIPERIOD ENERGY SYSTEMS

The objective of this project has been to develop computational strategies for solving multiperiod mixed-integer linear programming (MILP) synthesis models. We have considered the optimal design and operation of utility plants, as well as the optimal design and operation of oil platforms.

For the optimal multiperiod operation of utility systems it is assumed that an existing utility plant is given, as well as a number of time periods in which individual demands for steam and power can vary. The problem is to decide which equipment to turn on and off accounting for the changeover costs, which preclude that this problem be simply solved independently for each time period. The other complication that arises in this multiperiod MILP model is that because each time period involves 0-1 variables, standard decomposition techniques such as Benders decomposition cannot be applied. We developed a strategy that is based on the idea of transforming the multiperiod problem into a shortest-path problem (Iyer and Grossmann, 1997a). The idea is to generate according to some criterion several MILP solutions at each time period, which are then linked

accounting for the changeovers. This in effect is equivalent to synthesizing a network such as the one shown in Fig. 1 in which the optimal solution is found by a shortest path algorithm. Since it is in general not possible to generate the network once and for all, the procedure is iterative in nature involving an implicit enumeration scheme.

We applied this method to a 12 period problem of a utility plant with 2 boilers and 2 turbines and with the possibility of purchasing steam and electricity (Fig. 2). If the problem is solved as a single MILP it involves 204 0-1 variables, 721 continuous variables and 1053 constraints. This model could not be solved to optimality after 1 hour of CPU time with OSL. Instead, with the proposed method, the solution of 369 small MILP subproblems were required (17 0-1, 53 continuous, 103 constraints). The computation requirement for solving the problem to optimality was 5 minutes. While the cost savings were modest (3%) what is perhaps more significant is the nature of the solution. If the problem is solved independently for each time period, there are 25 predicted start-ups and shut-downs as seen in Fig. 3. With the simultaneous model there are only 5. Furthermore, while in the former there are 11 distinct period of operation, in the latter there are only 3!

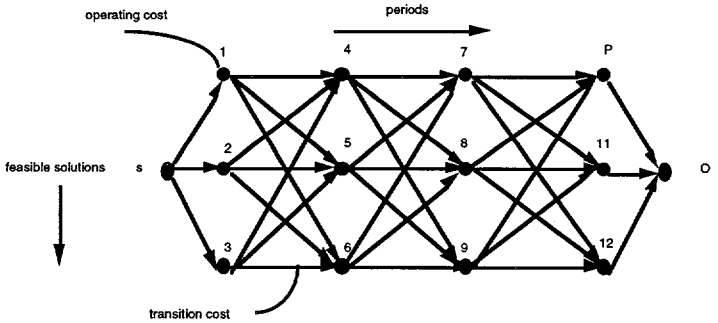

Fig. 1. Network representation of multiperiod operation

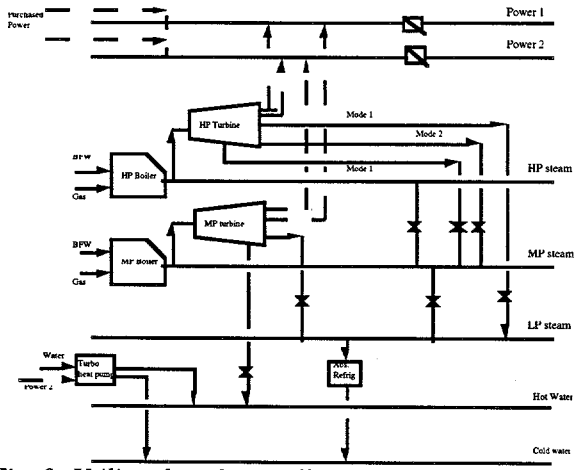

Fig. 2. Utility plant for small example.

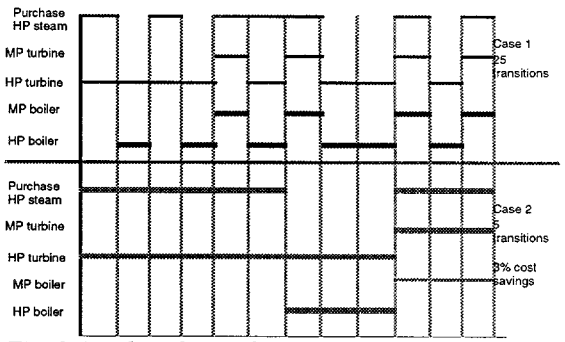

Fig. 3. Predicted shut-downs for independent optimizations (Case 1) and for simultaneous optimization (Case 2).

We were able to extend the above problem to include both synthesis of the utility configuration as well as the operation over multiple time periods (Iyer and Grossmann, 1997b). In addition, we also considered as part of the problem that each unit must be shut down at least at one period in order to perform maintenance. The complication in this problem lies on the fact that it gives rise to a large scale MILP that is very difficult ad expensive to solve. Schemes such as Generalized Benders or aggregation methods proved to be unsuccessful. Therefore, we developed a special bilevel decomposition method that consists of two levels: design problem, and operational

problem. The design problem corresponds to a relaxation that only involves 0-1 design variables since the 0-1 variables for each time period are eliminated, as well as the required lower bounds of activity for feasible operation. The operational problem arises with fixed 0-1 design variables, and gives rise to a problem almost identical to the one in the previous paragraph. The design problem predicts lower bounds while the operational problem predicts upper bounds. These two subproblems are solved successively by adding integer cuts and new design variable cuts to the design problem. We were able to demonstrate that this method is significantly faster than using a full space branch and bound enumeration. We also applied this method to a problem supplied to us by Mitsubishi Chemical in which we were able to predict large savings compared to a suboptimal solution obtained from the full space branch and bound method. It should be noted that we developed a similar bi-level decomposition solution approach for the multiperiod capacity planning and selection of process networks (Iyer and Grossmann, 1998a).

In cooperation with Mobil Oil, we also worked on the problem that deals with the optimal capacity selection of production and well platforms, and the scheduling of drilling of oil wells (see Fig. 3). This problem is also multiperiod in nature and has the added complexity that the description of the flow of the extracted crude is rather complex as it is nonlinear, and a function of the number and position of wells. We were able to develop a simplified MILP model by using piecewise linearizations. Since the multiperiod MILP model is quite large we developed a sequential hierarchical decomposition strategy that provide good suboptimal solutions (Iyer et al, 1998b). The basic idea relies on aggregating the time periods and the wells involved in a production field to define a higher level design problem that predicts an upper bound to the net present value. This model is used to select the wells that are to be exploited of the given time horizon. The problem is then disaggregated into selected wells and actual time periods, but solved in a rolling time fashion. This subproblem then defines the selection of platforms and their capacities. Finally, an optional subproblem is considered to "smooth" the production profiles (i.e. monotonic decrease) which then yields the final schedule. The quality of the solution can be assessed with the predicted upper bound. This decomposition strategy was applied to smaller test problems as well as to a real world problem. In the small problem, where we could also solve the MILP in the full space with CPLEX, the predicted optimum from our procedure was virtually identical. In the various problems the difference between the upper bound and the predicted solution was about 9%.

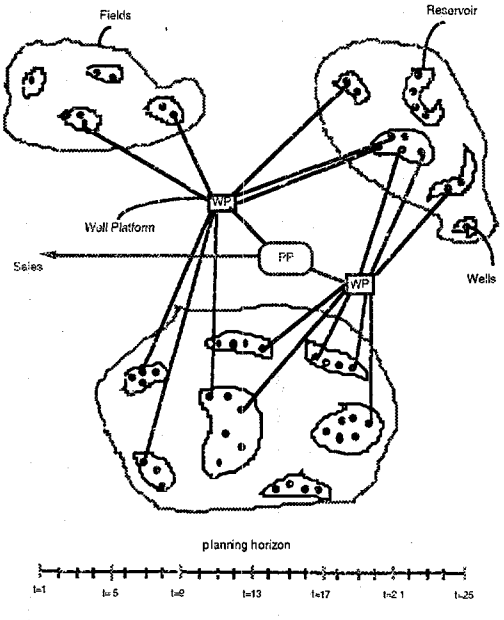

Fig. 3. Oilfield platforms and wells.

SIMULTANEOUS DESIGN, SCHEDULING AND DYNAMIC OPERATION OF BATCH PROCESSES

An important task for process optimization is the integration of multiple objectives, tasks and subsystems for a process. For design, these include trade-offs with the efficiency of raw material conversion, capital cost and energy consumption. In addition to profitability, performance interactions should be considered that include controllability, safety and tolerance to uncertainties, both with the process model and process disturbances. Finally, in process planning, there are interactions with other processes and trade-offs in considering demands and capacities as well as expansions and long range outlooks. Process optimization formulations naturally and directly handle interactions, multiple conditions and trade-offs in an unambiguous, quantitative manner. On the other hand, the resulting formulations may lead to more difficult problems to solve. Therefore it is very important to determine: a) which large-scale algorithms, software and hardware are available, b) what are the best problem formulations, and c) what further algorithmic development is needed.

Over the past decade a number of optimization formulations have been developed to integration of batch process design and scheduling (Birewar and Grossmann, 1989; Voudouris and Grossmann, 1993) and design and dynamic performance (Logsdon and Biegler, 1993). We have considered the design, operation and scheduling of a batch process. In particular, we are interested in results from nonintegrated design and optimization formulations and the impact of integrated formulations. By combining these problem aspects, we hope for synergies that lead to shorter processing times, shorter planning horizons and fewer, higher quality batches. Two important aspects to this case study are the use of simultaneous dynamic optimization and a simplified closed-form scheduling formulation.

For the simultaneous dynamic optimization we discretize the differential equations (DAEs) and state and control profiles to form a large-scale optimization problem. This approach handles profile constraints and incorporates equipment design variables directly. The resulting formulation works well even for unstable systems and the DAE model is solved only once during the optimization. The closed form scheduling formulation is adapted from Birewar and Grossmann (1989) and deals with the sequencing of tasks, products and equipment using simplified Unlimited Intermediate Storage (UIS) and Zero Wait (ZW) transfer policies. In both cases, a nonlinear program is formulated and the solution directly yields a minimum cycle time operating schedule for multiple products and stages. The detailed integrated formulation is given in Bhatia and Biegler (1996a). To demonstrate this approach we considered the process example given in Figure 4, consisting of a reactor, heat exchanger, centrifugal separator and batch column. We consider the sequencing of three products (P) of varying purity and with possible manipulations of the temperature profile in the reactor and the reflux profile in the column. We term the optimal dynamic profile cases R1 and C1 for the reactor and column, respectively. The best constant profile cases are termed R0 and C0. We also consider three profit maximization cases. First, we consider the *sequential design* where designs, dynamics and scheduling are optimized in sequence. The *intermediate case* deals with the final time states fixed by a unit optimization and then solution of a simultaneous design and scheduling. Finally, we consider a *fully simultaneous approach* with optimized final states. The optimal dynamic and constant profiles can be found in Bhatia and Biegler (1996a). The results of this case study are summarized in Figure 5 for the ZW case. Note that significant improvements result from the integrated formulation. Here we see that there is improvement due to a variable reflux ratio (from C0 to C1) but the greatest improvements are due to the integration of the design, operation and scheduling steps. The reason for this is apparent from the production schedule. The sequential solution still has long cycle times and long slack times in the ZW schedule. The intermediate solution reduces both of these considerably and the fully simultaneous approach eliminates the slack times altogether and creates a schedule with the shortest cycle time. This allows for much greater equipment utilization and significantly improves the profit.

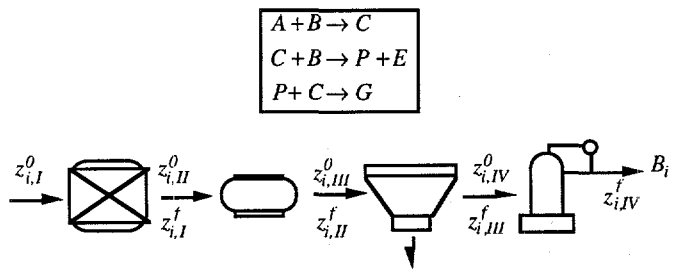

Fig. 4. Example of batch process

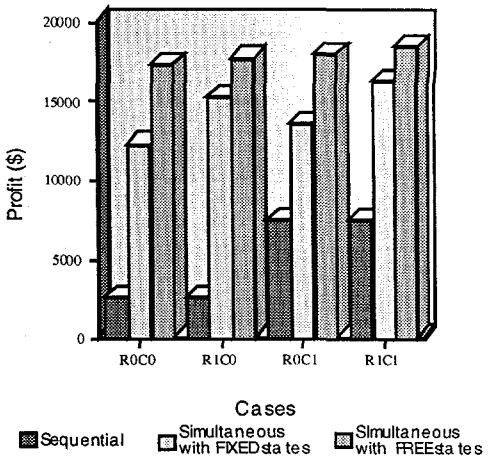

Figure 5: Results of Case Study for the ZW case

These results were obtained with the assumption of perfect operating and design models. Frequently, uncertainty in these models can easily offset some of the gains accomplished through integrated formulations. These can arise from an imperfect model and model parameters, process disturbances and uncertain inputs, and from variations in demands and supplies in planning. Nevertheless, treating uncertainty can also be handled through optimization formulations. Whether the uncertainty exists in the model or through disturbances, these are frequently not known in advance. To deal with realistic problem formulations we can consider a *robust (Here and Now or RI) formulation* which ignores variations in the controls or a *perfect information (Wait and See or PI) formulation* which assumes θ is known and cannot be implemented. Clearly, the latter formulation leads to a better objective and we can define an expected value of perfect information as: EVPI = y_{RI} - y_{PI}. An implementable intermediate strategy uses feedback correction (FC) whereby the control profiles are determined through variations in the state variables, i.e.: $u_i = u_{nom} + k (y_i - y_{nom})$. Here we can show that: y_{RI} y_{FC} y_{PI} and the feedback correction strategy can recover some of the EVPI. In Bhatia and Biegler (1996b) multiperiod formulations were solved for the above batch problem with uncertainties in the rate constant and relative volatility. For the ZW case the feedback correction strategy recovers about 90% of the EVPI. The challenge in considering process uncertainty lies in the inexpensive solution of multiperiod optimization problems. Varvarezos et al. (1992) developed an efficient decomposition strategy that was linear in the number of periods and was easily parallelized. More recently, Bhatia and Biegler (1997) developed an Interior Point method for multiperiod problems which helps preserve problem structure structure and speed convergence. Again, the decomposition is linear in number of periods and each period can be solved in parallel. Moreover, with enough processors, the cost of a multiperiod design could be that of a single optimization.

SYNTHESIS OF FLEXIBLE SEPARATION PROCESSES

We have investigated the synthesis of a solvent recovery utility support systems for several processes located at a single plant site. For this problem we wish to synthesize a flexible separation process. We limit our investigation to the use of distillation-based technology to effect the separations. A goal is synthesize an industrial process where the research issues include the need to overcome problems that arise because of the scale and complexity of the problem.

The problem is to synthesize a separation process to recover solvents from a mixture of solvents coming from several processes sharing the same plant site. The feed to the desired separation process varies during the year. We assume the feed will be fixed for a period of time (a few days to a few weeks) and then will change significantly in flow and composition as one of the processes on the site changes in its operation -- e.g., it might shut down for a while or it might start

processing a different feed stock. We assume we can predict the different representative feeds and their duration throughout the year. We illustrate by assuming the solvents are acetone, chloroform and benzene (ACB). Fig. 6 is a composition diagram showing five different feed compositions we might wish to process over the course of a year. Solvents selected for a process are generally very dissimilar in nature. As such, mixtures of them will display azeotropic and liquid/liquid behavior. The ACB phase diagram at one atmosphere displays a maximum azeotrope between acetone and chloroform and a curved "distillation boundary" running from that azeotrope to the benzene corner. There are many aspects to this synthesis problem that make it very difficult. We discuss each in turn. Fig. 7 shows a separation process capable of separating the first feed shown in Fig. 6 into pure component products. Typical of separating azeotropic mixtures, one finds the need for recycles. We have readily enumerated three different configurations to separate feed 1. Each of the other feeds has several different separation schemes possible.

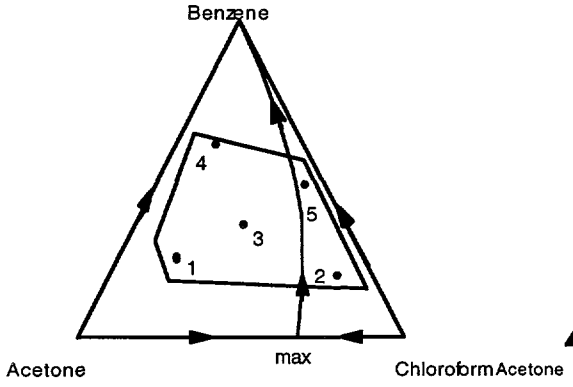

Fig. 6. Composition diagram for acetone, chloroform and benzene mixtures diplaying different feeds expected throughout a year of operation for a solvent recovery system

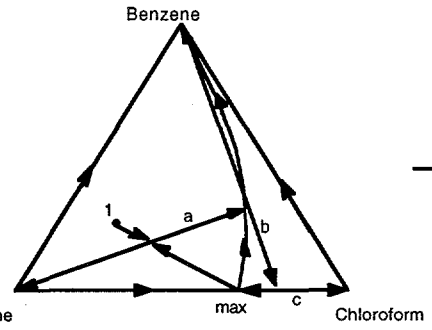

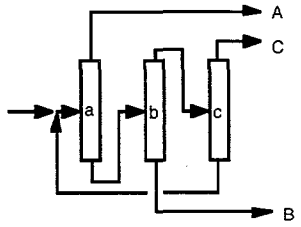

Fig 7, One of several separation schemes for processing feed 1

Suppose we have decided on the configuration we intend to use for separating each of the feeds. Suppose further that each has three columns in it. Since each of the feeds occurs at a distinct time, we can consider sharing equipment among these configurations. For example, suppose we have to process feed 1 during January. During February and March we have to process feed 2. Suppose both require three columns in their respective design configurations. There are many ways we could share equipment between these two configurations. For example, we could have six different columns. Or we could use column 'a' for feed 1 as column 'c' for feed 2 if it were designed appropriately (adequate number of trays, large enough diameter, designed for the pressure needed, etc). There are 120 ways to share these columns (e.g. (a,b,c)(d,e,f); (a,b,c)(a,e,f); (a,b,c)(d,a,f), ...) For four feeds with each design configuration requiring four columns, the number of design alternatives is over 60,000. With six columns and four feeds, the number grows to 1.7 million.The design of such processes could involve the saving of intermediates (e.g., the azeotropic mixture which is the distillate for column 'c' in Fig. 7) to be processed with a different feed at a different time. When we do, the number of alternatives explodes even more.

In the course of evaluating each of the columns in a design, we need to simulate a column. When mixtures to be separated display azeotropic and liquid/liquid behavior, they become markedly more difficult to simulate. Simulations using commercial distillation packages often fail. For example, consider column 'b' in Fig. 7. Its feed is in the distillation region to the left of the distillation boundary while its products are both in the distillation region to the right of the boundary. Unless one knows in which region the products will reside, it can be extremely difficult to make an initial guess for the simulation that can converge. Thus we should expect even when we propose a column as a part of a design, we may have difficulty in simulating it to discover how best to design

it and estimate a cost for it. The column does not operate alone but rather within a system of columns having recycles of one or more of the intermediate and final products within it. Converging a simulation model for a system of columns, each difficult when simulating on its own, and having recycles among them is even more difficult. We then add the desire to optimize such a process.

The number of trays in each of the column sections is an integer quantity which affects the simulation if we carry it out using tray by tray calculations. We have to add these to those variables we might use to select among the sharing and configuration alternatives we mentioned above. We have an extremely large mixed integer highly nonlinear optimization problem to solve which is highly prone to numerical failure while trying to solve. There are several approaches for solving problems of this type. One is to use methods like simulated annealing or genetic algorithms. These methods handle both discrete and continuous variables. However, these methods take thousands to tens of thousands of iterations. We choose not to afford such a large computational burden for our problem, which we have shown above is extremely large and difficult. We have considered the use of branch and bound methods to handle the search over the configuration decisions. We have identified computations that establish bounds on costs for such processes to make branch and bound methods effective. For example, we will compute a bound on the cost of a column in a configuration of columns by optimizing the configuration and having only the cost of that column as the objective function. A similar lower bound on utility cost for a column is also possible. These are not trivial computations to establish bounds, but, when they allow one to remove many of the designs possible from consideration, they should prove effective. We are also looking at using simplified models. The first is the use of collocation models for distillation columns. Collocation models convert the discrete variables characterizing the number of trays into continuous variables, a distinct advantage. These models also do not get larger for difficult separations as the model size reflects the order of the polynomials used to collocate and not the number of trays. Our collocation model is about the size of tray-by-tray models involving 18 trays for three component mixtures.

We are also developing simplified models of the composition space and its distillation boundaries. Such models are allowing us to develop very quickly material balance models for systems of columns having recycling intermediate and final products. When using these models, we are discovering even more design alternatives we overlooked previously. To search the enormous space of alternatives, we are developing a solution approach based on using so-called asynchronous teams (A-teams) of agents. Developed in the early 1980s at Carnegie Mellon in the Electrical and Computer Engineering department by Talukdar and his students, industry has used A-teams to solve several of their very large optimization problems effectively (circuit routing for VLSI, train rescheduling, and asynchronous traveling salesmen problems).

A-teams are teams of cooperating agents which attack the problem in parallel - rather like a colony of insects attacking a large systems problem such as building a home or finding and storing food. There are various agents doing different tasks. Each has a relatively simple and well-defined task. There are simulator agents, optimizer agents, heuristic configurers, destroyers, and so forth. They are autonomous because they decide when to run and on which problem to work. The only exchange of information among the agents is their sharing of their partial and complete solutions with each other. An example is to have several optimizers, one based on a genetic algorithm, another which is a hill climber, and a third which employs a branch and bound scheme to search over discrete decisions. The genetic algorithm will put solutions all over the solution space; thus it is very good at getting coverage of the space when optimizing. However, it is terribly slow to converge to a local optimum. The hill climbing algorithm can use good points generated by the genetic algorithm and march them to a local minimum. The branch and bound algorithm can take the better solutions found by any of the other algorithms and use them as upper bounds on the cost to trim the branches it has to search. The genetic algorithm can employ some of the solutions found by the others as parents from which to generate its next set of "children." Experience shows that A-teams often solve problems many times faster (100 times faster is not uncommon) and generally

find better solutions than any of the algorithms used by any of the agents from which they are composed. A-teams cannot promise to find global optimal solutions, but they often find very close to global optimal solutions for a number of test problems. We will be building our agents using the ASCEND modeling environment to carry out the simulation and continuous variable optimizations needed. By next year we will complete our study and intend to have created an A-team having agents capable of synthesizing the better solutions for separating a flexible solvent recovery system. We expect to have illustrated this system in solving at least two different solvent recovery problems.

CONCLUSIONS

This paper has given an overview of recent optimization approaches that we have developed for solving a variety of multiperiod optimization problems for process design and process operation that range from utility systems and oilfields, to batch processes and distillation systems. The results that have emerged from the projects in the three application areas indicate that the keys to successful solution to these large-scale optimization problems are decomposition, modeling and hybrid solution methods.

ACKNOWLEDGMENT

The authors gratefully acknowledge financial support from DOE under Grant No. DE-FG02-85ER13396.

REFERENCES

Bhatia, T. K. and L. T. Biegler, "Dynamic optimization in the design and scheduling of multiproduct batch plants," I & EC Research. 35, 7, 2234 (1996a)

Bhatia, T., and L. T. Biegler, "Dynamic Optimization in Planning Under Process Model Uncertainty," submitted for publication (1996b)

Bhatia, T. K. and L. T. Biegler, "Multiperiod design and planning with interior point methods," presented at Annual AIChE meeting, Los Angeles, CA (1997)

Birewar, D. and I. E. Grossmann, "Efficient algorithms for the scheduling of multiproduct batch plants," I & EC Research, 28, p.1333 (1989)

Iyer, R. and I.E. Grossmann, "Optimal Multiperiod Planning of Utility Systems", *Computers and Chemical Engineering* , **21**, 787-800 (1997a).

Iyer, R. and I.E. Grossmann, "Synthesis and Operational Planning of Utility Systems for Multiperiod Operation", accepted for publication, *Computers and Chemical Engineering* (1997b).

Iyer, R. and I.E. Grossmann, "A Bilevel Decomposition Algorithm for Long Range Planning of Process Networks," *Ind.Eng.Chem. Res.* , **37**, 474-481 (1998a).

Iyer, R. and I.E. Grossmann, "Optimal Planning and Scheduling of Offshore Oil Field Infrastructure Investment and Operations," *Ind.Eng.Chem. Res.*, **37**, 1380-1397 (1998b).

Logsdon, J. S. and L. T. Biegler, "Accurate determination of optimal reflux policies for the maximum distillate problem in batch distillation," I & EC Research, 32, 4, p. 692 (1993)

Varvarezos, D., L. T. Biegler and I. E. Grossmann, "Multiperiod design optimization with SQP decomposition," Comp. Chem. Engr.,18, 7, p. 579 (1992)

Voudouris, V. T., and I. E. Grossmann, "Optimal synthesis of multiproduct batch plants with cyclic scheduling and inventory consideration," I & EC Research, 32, 2, p. 1962 (1993)

Issues Involved with Non-Characterized Control of Methanotrophic Bacteria

Daphne L. Stoner, Charles R. Tolle, Karl S. Noah, Dennis A. Davis, Karen S. Miller, and Dee Jay Fife *

Idaho National Engineering and Environmental Laboratory
P.O. Box 1625
Idaho Falls, ID 83415-2210, USA

May 11, 1998

Abstract

Methane-utilizing bacteria, methanotrophs, have application as biocatalysts in the commodity chemical production, waste treatment and environmental remediation industries. Methanotrophs have the ability to oxidize many chemical compounds into more desired products, such as the production of propylene oxide. Methanotrophs can also degrade toxic compounds such as trichloroethylene. However, there are many physical, chemical and biological problems associated with the continuous oxidation of chemicals. These include, low mass transfer of methane, oxygen and propylene; toxicity of substrates and degradation products, and competition between the growth substrate, i.e., methane and chemical feed stock, e.g., propylene for the biocatalyst. To supervise methanotrophic bioprocesses, an intelligent control system must accommodate any biological limitations, e.g., toxicity, and mitigate the impact of the physical and chemical limitations, e.g., mass transfer of methane and the solubility of propylene. The intelligent control system must have the capability to assess the current conditions and metabolic state of the bacteria; recognize and diagnose instrument faults; and select and maintain sets of parameters that will result in high production and growth.

1 INTRODUCTION

Methanotrophs are microorganisms that derive the carbon and energy required for growth from the metabolism of methane [6], [8], [11], [19]. The ability to oxidize and grow on methane is due to methane monooxygenase (MMO), a large multicomponent enzyme [17]. The broad substrate specificity of MMO allows the use of methanotrophs for such diverse applications as commodity chemical production, waste treatment and environmental remediation. Potential uses for methanotrophs in the commodity chemical industry include the production of methanol, alkene epoxides [21] such as propylene oxide and polyhydroxybutyrate (PHB) [14], [13]. Propylene oxide is used in the preparation of polyethers (used to form polyurethanes) or propylene- and dipropylene glycols [20]. PHB, a storage polymer synthesized by methanotrophs under

*This work is supported by the U.S. Department of Energy, Office of Energy Research, Office of Basic Energy Sciences, under DOE Idaho Operations Office Contract DE-AC07-94ID13223.

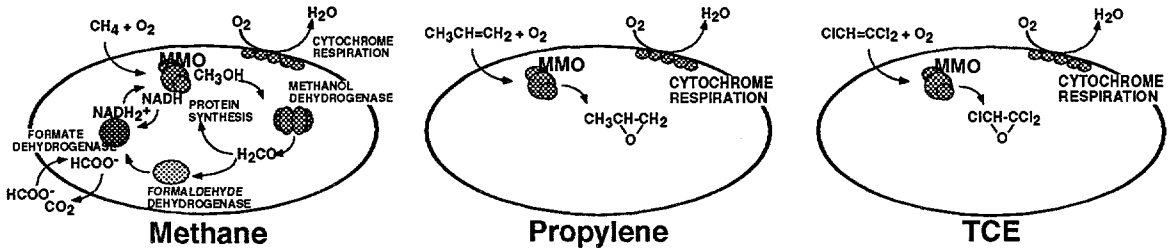

Figure 1. Methanotroph ($OB3b$) Substrate Competition.

conditions of nitrogen limitation, can be applied to the production of biodegradable plastics [5].

The cultivation of methanotrophs in a continuous stirred tank reactor for commodity chemical production presents a number of interesting control challenges. The main challenge is due to the fact that microbial activity cannot be controlled directly. Microbial activity can be influenced by manipulating and controlling the physical and chemical environment of the microorganism. In a continuous process of methanotrophic bioconversion, the process must be supervised in such a manner as to allow the gowth of bacteria and regeneration of catalyst (MMO) and electron donor ($NADH_2^+$),all the, while meeting process goals of modified chemicals. There are physical as well as physiological limits to any bioprocess, only some of which can be mitigated or improved upon by closely coupled control systems.

2 CONTROL ISSUES

2.1 Providing Methane, Oxygen, Nitrogen and Carbon Dioxide

Because growth on methane requires introduction of a gaseous carbon substrate, bacterial growth may be limited by the rate at which methane is transferred from the gas phase into the liquid culture medium. Intelligent control will allow close integration of the growth and catalysis requirements of the process with the addition of methane to the system. Continuous control of methane introduction and mixing speed will allow these to be varied in order to sustain maximum transfer efficiency for methane regardless of feed rates, temperature, and amount of biomass. Minimizing methane in the gas outlet while still introducing it into the liquid medium implies that methane concentrations within the bioreactor fluid will be at or near growth-limiting concentrations.

In addition to methane, oxygen is required as an electron acceptor for the energy yielding reactions of aerobic respiration and for the oxidation of methane to methanol by MMO[12], see Figure 1. Oxygen can be supplied as a component of air or as a separate controllable gas stream. There exists an optimal balance. Too low a dissolved O_2 level will result in decreased growth and chemical oxidation rates. Too high an O_2 level which results from continuous sparging with pure O_2 can result in dissolved O_2 concentrations that are toxic. Using intelligent control, the O_2 supply can achieve this balanced within the requirements of the process.

Methanotrophic bacteria have an apparent requirement for CO_2 [18] that may or may not be satisfied by atmospheric CO_2, in the early stages of growth, or CO_2 produced by carbon metabolism [21]. It has been shown that, supplementing batch cultures with CO_2 supplied as a gas or bicarbonate during the lag phase significantly shortens this phase of growth[21].

2.2 Substrate Competition/MMO Substrate Specificity

The oxidation of the broad range of compounds by methanotrophs occurs by co-metabolism. That is, these compounds are oxidized by the fortuitous action of MMO and do not support the cell's carbon or energy requirements. When cultivated on methane, there is competition between methane and the material being oxidized, i.e., propylene, for the active site of MMO. To sustain a continuous treatment process, the microorganisms' carbon and energy requirements must be continually met, but excess growth substrate cannot interfere with the reaction of interest. Overall, the requirements or productivity standards for an economic bioprocess must be balanced with the growth requirements of the microorganism. With this in mind, we propose a balanced cost function which mathmatically state the competition:

$$P = f\, P_{biomass} + (1-f)\, P_{methane} \tag{1}$$

where,

$$P_{biomass} = Optical\ Density \tag{2}$$

$$P_{methane} = \frac{3}{methane + 1} \tag{3}$$

$$f \in [0,1] \tag{4}$$

$$Optical\ Density \in [0,3] \tag{5}$$

$$methane \in [0,1]. \tag{6}$$

2.3 Providing Reducing Power and Oxygen for Catalysis and Growth

The activity of MMO requires an electron donor (reducing power or reducing equivalents) which is provided by reduced $NADH_2^+$. During growth on methane, the $NADH_2^+$ is regenerated [6], [13], [1]; however, during the co-oxidation substrates $NADH_2^+$ is not. Thus, during co-oxidation there is a finite transformation capacity in the absence of a supplemental energy supply.

For cometabolic reactions mediated by MMO, formate or methanol can be used as an energy source. However, methanol is toxic to the microorganism and can significantly affect microbial activity if concentrations exceed inhibitory levels.

Reducing power in the form of intracellular H_2 can be generated when the cells are growing using atmospheric N_2 as a nitrogen source [22], [13], [15]. Unfortunately, growth using atmospheric nitrogen is an energy intensive process generally resulting in significantly decreased growth rates [10]. Growth of M. trichosporium $OB3b$ on N_2 is also apparently O_2 sensitive; no growth is observed when cells are inoculated directly into nitrate-free medium [16]. In order to prevent sensitivity to O_2, intelligent control may allow improved yields by more closely coupling the O_2 levels with what is required by the microorganism. Control systems may also improve the cycling between growth on nitrate to keep cell numbers high, and growth on N_2, which would generate intracellular H_2 for co-metabolism.

2.4 Eliminate, or Minimize, Inhibitor Effects

The inhibition of growth by accumulated products such as methanol [15] or propylene oxide [13] is a control issue for commodity chemical production. In addition to substrate and product toxicity, aeration in the absence of a suitable substrate may produce a MMO-oxygen activated

Table I
Physical, chemical, and biological characteristics of methane, propylene, propylene oxide, trichloroethylene, and trichloroethylene oxide.

	Compound				
Characteristic	Methane	Propylene	Propylene Oxide	Trichloroethylene	Trichloroethylene Oxide
Phase	Gas	Gas	Liquid	Liquid	Liquid
Volatile	Yes	Yes	Yes	Yes	Yes
Water Solubility	Low	Low	Medium	Low	Medium
Bacterial Toxicity	No	No	Yes	Yes	Yes
Human Toxicity	No	No	Yes	Yes	Yes

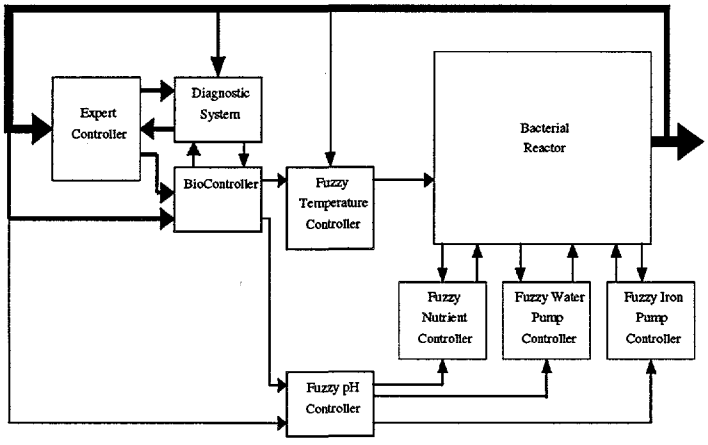

Figure 2. Control system block diagram.

species that is toxic to the cells [1]. Note that the mode of inhibition has not been identified as of yet.

Propylene also competes with methane for the active site on MMO. Propylene, a gas, is sparingly soluble while propylene oxide is moderately soluble in water Table I(Table 3). The low solubility of the substrate is a physical limitation that can affect bioconversion rates, while the accumulation of propylene oxide in the bioreactor fluid presents a control problem because of the toxicity of this compound to the microorganisms.

3 CONTROLLER CONCEPT

3.1 Intelligent Control of the Continuous Cultivation of Methanotrophs

A hierarchical control system is being developed and applied to the cultivation of *Methylosinus trichosporium OB3b* in a continuous stirred tank reactor, see Figure 2. The top level consists of an expert controller integrated with a stochastic learning algorithm. Furthermore, the expert

controller will be based on a supervisory shell that will be developed using expert knowledge and the history of the reactor operation to determine the set points that will be required to meet a production criteria. This supervisory shell will analyze the data, determine the current state of the system, and recommend and implement the set points required to optimize reactor performance based on Equation 1. The second level will be a diagnostic system that uses expert knowledge to determine the operational status of the sensors and actuators, to monitor liquid delivery rates, and to recalibrate the pumps when deviations from desired flow rates occur. When detected, equipment malfunctions will be logged to a data file and the operator notified by the diagnostic system. This subsystem watches over the bioreactor fitted with a variety of sensors, stirrer, and aeration, gas sparging, temperature control, liquid feed, and pH control systems. The hardware is interfaced with a computer based control system comprised of a number of lower level control modules. This lowest level of the hierarchy will be implemented as a number of integrated set point controls and data acquisition modules. The unified control system will determine the optimum conditions for the cultivation of the methanotroph, *Methylosinus trichosporium OB3b*. Growth on nitrate or N_2 as the source of nitrogen, as well as the use of N_2 reduction with nitrogenase to produce intracellular H_2 and hydrogenase to regenerate reducing power ($NADH_2^+$), will be evaluated.

3.2 Intelligent Control of the Methanotrophic Conversion of Propylene to Propylene Oxide

The supervisory control system developed for the cultivation of methanotrophs will be modified to allow the production of propylene oxide. This modification has already been planned for as an integral part of the cost function in Equation 1. For the biological conversion of propylene to propylene oxide, the supervisory control system must balance the physiological requirements for the maintenance of significant levels of MMO and the process requirements for efficient production. The major physiological considerations for controlling a continuous process for the conversion of propylene to propylene oxide are: 1) the oxidation of propylene is a co-metabolic process; and 2) the product, propylene oxide, is toxic to the microorganism. The main physico-chemical limitations of this process are the low solubility of the gaseous substrate and the moderate solubility of the product. To maximize productivity of the bioreactor, propylene must be efficiently transferred from the gas phase into the liquid phase and the product must be continually removed to maintain concentrations below inhibitory levels.

One control scenario that may minimize the competition between methane and propylene for the active site of MMO is to alternate introduction of these gases into the bioreactor. In this system, the supervisory control system will evaluate the cycling of these gases as a means to improve the overall productivity of the bioreactor and to achieve biotransformation capacities that are attainable in non-competitive batch transformation [14]. The periodicity with which the gases are added may be best determined using a stochastic learning procedure. A second strategy for improving yields is cycling the operating temperature of the bioreactor between the temperature required to remove propylene oxide from solution and that required for optimal growth of the microorganism. Operating a bioreactor at an elevated temperature was used to minimize the accumulation and, thus, toxicity of propylene oxide in a bioprocess [13]. The Supervisory Control System will use expert knowledge to evaluate methods to replenish reducing power continually by manipulating the H2-generating nitrogenase or by the addition of methane, methanol, formate, or other energy-yielding compound.

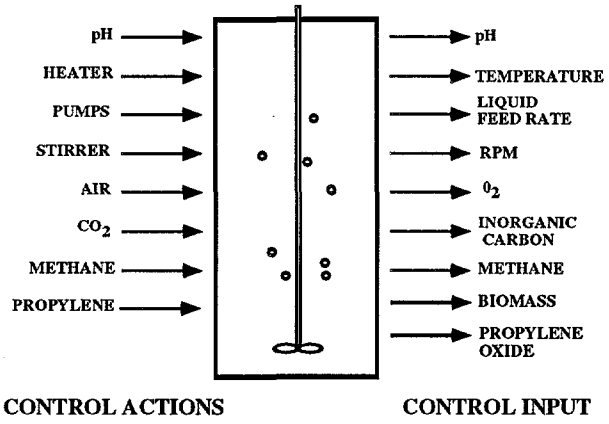

Figure 3. Reactor sensing and detection techniques.

4 A CLOSER LOOK INTO THE CONTROL SYSTEM

4.1 Supervisory Control System

The initial goal of the Supervisory Control System will be optimization of the productivity of the bioreactor, i.e., the production of biomass. The amount of biomass will be assessed on-line via optical density using an on-line biomass sensor that works like a spectrophotometer. The Supervisory Control Program includes the identification of state using expert knowledge, a stochastic learning procedure to determine optimum operating parameters, and control strategy based on expert knowledge. The system will also include a means to supervise direct control, communicate with an operator, and interface with the Diagnostics Program.

4.2 Diagnostics Program

Hardware performance will be monitored; any failures detected will be recorded by the equipment diagnostics program. The diagnostics program will read sensor and set-point data and determine whether the data are consistent with the desired system operation. The Diagnostic System will record changes in set points and allow the operator to log messages manually. The Diagnostics Program will be integrated with the supervisory control system, to allow for corrective actions to take place.

4.3 Details of the Lower Level and Feedback Control Systems

The lower level control system is an integrated system of sensors, actuators, and data acquisition modules that monitor and provide set point control of the nutritional and environmental state of the bioreactor. This system will be used to control O_2, CO_2, methane, and N_2 concentrations. While O_2, CO_2, and N_2 requirements are likely to be met by air, provisions have been made for supplementing these gases through separate, controllable gas mass flow controllers. Methane will be supplied as a separate, controllable gas stream. System state observations will be accomplished by on-line and off-line techniques, shown in Figure 3. On-line sensors will be used to assess dissolved O_2 and CO_2 within the bioreactor fluid, while inlet and outlet concentrations of N_2, methane, O_2, and CO_2 will be determined by on-line gas chromatography. On-line biomass estimations will be made by an optical density probe.

Nutrient salts solution will be used to provide phosphate, sulfate, iron (Fe), nickel (Ni) and molybdenum (Mo). Nutrient feed rates will be controlled by a self-calibrating pumping system interfaced with the pH control system. The pH of the culture medium will be maintained automatically with a pH control system using an acid and a base pumping system; the phosphate provided within the nutrient feed will buffer the system. Temperature will be maintained through a close loop controller, using an internal temperature probe for on-line measurement of fluid temperature and an external heating blanket for maintaining the temperature at the set point.

5 SUMMARY

In summary, an intelligent control system for the production of propylene oxide by methanotrophic bacteria can only control microbial growth and metabolism indirectly by manipulating and controlling the physical and chemical conditions. Thus, the control system must: control the rate and improve the efficiency in which the gaseous substrates methane and oxygen is introduced into the liquid phase and utilized by the bacteria; closely couple growth with commodity chemical to maintain biocatalytic efficiency; select the sets of conditions, e.g., pH, temperature, nutrient concentration that will result in optimal growth and commodity chemical production. The intelligent control system must have the capability to assess the current conditions and metabolic state of the bacteria; recognize and diagnose instrument faults; and select and maintain sets of parameters that will result in high production and growth.

ACKNOWLEDGMENTS

The authors would like to acknowledge Dr. John Johnson and Eric Larsen for their work considerable work on previous portions of this ongoing research.

References

[1] Alvarez-Cohen, L., and P. L. McCarty. "Effects of toxicity, aeration, and reductant supply on trichloroethylene transformation by a mixed methanotrophic culture," Appl. Environ. Microbiol. vol. 57, 1991, pp. 228-235.

[2] Alvarez-Cohen, L., and P. L. McCarty. "Product toxicity and cometabolic competitive inhibition modeling of chloroform and trichloroethylene transformation by methanotrophic resting cells," Appl. Environ. Microbiol. vol. 57, pp. 1031-1037.

[3] Alvarez-Cohen, L., P. L. McCarty, E. Boulygina, R. S. Hanson, G. A. Brusseau and H. C. Tsien. "Characterization of a methane-utilizing bacterium from a bacterial consortium that rapidly degrades trichloroethylene and chloroform," Appl. Environ. Microbiol. vol. 58, 1992, pp. 1886-1893.

[4] Andrews, G. "Engineering Considerations," *In Biotechnology for the Treatment of Hazardous Waste*, D. L. Stoner (ed.) Lewis Publishers, Boca Raton, FL, 1994, pp. 157.

[5] Asenjo, J. A., J. S. Suk. "Microbial conversion of methane into poly-b-hydrodroxybutyrate (PHB): Growth and intracellular product accumulation in a Type II methanotroph," J. Ferment. Technol. vol. 64, 1986, pp. 271-278.

[6] Bédard, C. and R. Knowles. "Physiology, biochemistry, and specific inhibitors of CH4, NH4+, and CO oxidation by methanotrophs and nitrifiers," Microbiol. Rev. vol. 53, 1989, pp. 68-84.

[7] Bowman, J. P., L. Jiménez, I. Rosario, T. C. Hazen, and G. S. Sayler. "Characterization of the methanotrophic bacterial community present in a trichloroethylene-contaminated subsurface groundwater site," Appl. Environ. Microbiol. vol. 59, 1993, pg. 2380.

[8] Brusseau, G. A., E. S. Bulygina, and R. S. Hanson. "Phylogenetic analysis and development of probes differentiating methylotrophic bacteria," Appl. Environ. Microbiol. vol. 60, 1994, pp. 626-636.

[9] Chang, H.-L. and L. Alvarez-Cohen. "Biodegradation of individual and multiple chlorinated aliphatic hydrocarbons by methane-oxidizing cultures," Appl. Environ. Microbiol. vol. 62, 1996, pp. 3371-3377.

[10] Chu, K.-H., and L. Alvarez-Cohen. "Trichloroethylene degradation by methane-oxidizing cultures grown with various nitrogen sources," Water Environ. Res. vol. 68, 1996, pp. 76-82.

[11] Higgins, I. J., D. J. Best, R. C. Hammond, and D. Scott. "Methane-oxidizing microorganisms," Microbiol. Rev. vol. 45, 1981, pp. 556-590.

[12] Higgins, I. J. and J. R. Quayle. "Oxygenation of methane by methane-grown Pseudomonas methanica and Methanomonas methanooxidans," Biochem. J. vol. 118, 1970, pp. 201-208.

[13] Hou, C. T. "Propylene oxide production from propylene by immobilized whole cells of Methylosinus sp. CRL 31 in a gas-solid bioreactor," Appl. Microbiol. Biotechnol. vol. 19, 1984, pp. 1-4.

[14] Hou, C. T., R. N. Patel, A. I. Laskin, N. Barnabe. 1979. "Microbial oxidation of gaseous hydrocarbons: epoxidation of n-alkenes by methylotrophic bacteria," Appl. Environ. Microbiol. vol. 38, 1979, pp. 127-134.

[15] Oldenhuis, R., R. L. J. M. Vink, D. B. Janssen and B. Witholt. "Degradation of chlorinated aliphatic hydrocarbons by Methylosinus trichosporium OB-3b expressing soluble methane monooxygenase," Appl. Environ. Microbiol. vol. 55, 1989, pp. 2819-2826.

[16] Shah, N. N., M. L. Hanna, K. J. Jackson, and R. T. Taylor. "Batch cultivation of Methylosinus trichosporium OB3b: IV. Production of hydrogen-driven soluble or particulate methane monooxygenase activity," Biotechnol. Bioeng. vol. 45, 1995, pp. 229-238.

[17] Stirling, D. I., J. Colby and H. Dalton. "A comparison of the substrate and electron-donor specificities of the methane mono-oxygenases from three strains of methane-oxidizing bacteria," Biochem. J. vol. 177, 1979, pp. 361-364.

[18] Strøm, T., T. Ferenci, and J. R. Quayle. "The carbon assimilation pathways of Methylococcus capsulatus, Pseudomonas methanica, and Methylosinus trichosporium (OB3b) during growth on methane," Biochem. J. vol. 144, 1974, pp. 465-470.

[19] Whittenbury, R. K., K. C. Phillips, and J. F. Wilkinson. "Enrichment, isolation and some properties of methane utilizing bacteria," J. Gen. Microbiol. vol. 61, 1970, pp. 205-218.

[20] Windholz, M. Editor. *The Merck Index. Tenth Edition. An Encyclopedia of Chemicals, Drugs and Biologicals.* Merck & Co., Inc. Rahway, N.J., 1983, pp. 1131.

[21] Park, S., M.L. Hanna, R.T. Taylor, and M.W. Droege. "Batch cultivation of Methylosinus trichosporium *OB3B*. I: Production of soluble methane monooxygenase." Biotech. Bioeng., vol. 38, 1991, pg. 423.

[22] Henry, S. M. and D. Grbic-Galic. "Influence of endogenous and exogenous electron donors and trichloroethylene oxidation toxicity on trichoroethykene oxidiation by methanotrophic cultures from a groundwater aquifer." Appl. Environ. Microbiol., vol. 57, 1991, pp. 236-244.

MEASUREMENT OF ABSOLUTE METHYL RADICAL CONCENTRATION IN A HOT-FILAMENT REACTOR USING CAVITY RING-DOWN SPECTROSCOPY

T.G. Owano and C.H. Kruger

High Temperature Gasdynamics Laboratory
Department of Mechanical Engineering
Stanford University
Stanford, CA 94305-3032

ABSTRACT

Methyl radicals are generated in a hot-filament diamond synthesis reactor using a resistively heated tungsten filament (20 mm long) in a slowly flowing mixture of 0.5 % CH_4 in H_2. The UV absorbance of CH_3 is measured during deposition using cavity ring-down spectroscopy (CRDS). We observe a strong sensitivity of the methyl radical concentration throughout the reactor to the substrate temperature. At some operating conditions, we also observe the methyl radical concentration to peak at a location several mm from the filament surface. This behavior of CH_3 with distance from filament is in qualitative agreement with two-dimensional models of the deposition environment, and is attributed to the effect of Soret diffusion on the balance of the primary methyl production/destruction reaction. The near surface concentration of methyl is observed to increase linearly with increasing substrate temperature, and is found to increase and saturate with increasing filament temperature.

INTRODUCTION

The methyl radical has fundamental importance for studies of diamond film growth by chemical vapor deposition (CVD) because it is regarded as a gas-phase precursor of the diamond film.[1-3] Therefore, starting with the first report in 1988 on infrared detection of CH_3 during filament-assisted growth of diamond,[4] several techniques has been applied to monitor methyl radicals in a CVD reactor, including REMPI spectroscopy,[4-8] UV absorption spectroscopy,[9, 10] and mass spectrometry.[11] These techniques, however, can be intrusive (as in the case of REMPI) and of limited spatial resolution (mass spectroscopy) and sensitivity (absorption). The CH_3 mole fraction in a CVD reactor has been modeled,[12] and the relation between the model predictions and growth rate and film quality has been studied. [13, 14]

We have developed diagnostics for the methyl radical based on the cavity ring-down spectroscopy technique (CRDS).[15-20] CRDS is a highly sensitive absorption spectroscopy that determines the absolute absorbance of a laser pulse passing through a sample. In a manner

similar to single-pass laser absorption spectroscopy, this measurement is performed with two-dimensional spatial resolution; however, unlike the case of single-pass absorption spectroscopy, CRDS measures absorbance as low as 10^{-5} – 10^{-7} and is insensitive to shot-to-shot power fluctuations in the laser pulses. These features make CRDS suitable for high sensitivity measurements in the near UV spectral region where pulsed lasers are commonly used.

In this report we present measurements of the methyl radical, which provide absolute CH_3 concentration profiles in a hot-filament reactor. Our technique takes advantage of the high sensitivity measurement of methyl radical absorbance at 213.9 nm made possible by cavity ring-down spectroscopy. The CH_3 absorption cross-section (σ) at 213.9 nm has been measured by Hwang and coworkers,[21, 22] who found σ to be insensitive to gas temperature within the range of 1250 K to 2000 K. ($\sigma = 1.04 \pm 0.13 \times 10^6$ cm^2/mol)

EXPERIMENTAL FACILITY

The experimental setup for cavity ring-down spectroscopy of methyl radicals in a hot-filament reactor has been described in detail elsewhere.[23] In the present study, the ring-down cavity is 62 cm long with mirrors mounted in 1.5 inch thick aluminum blocks separated with four stainless steel rods 3/4 inch in diameter for cavity stability. The reactor is placed inside this cavity frame and connected to the mirror mounts by means of flexible bellows. A laser pulse injected into the cavity circulates back and forth along the same path between the cavity mirrors, crossing the reactor parallel to the filament and substrate. The distance between the filament and the pulse path is controlled with a micrometer that moves the reactor on a translation stage.

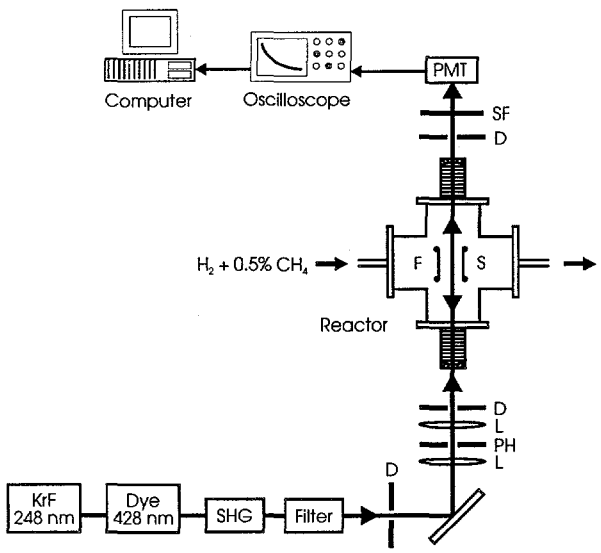

Figure 1. Schematic of the CRDS system and the hot-filament reactor. PMT = photomultiplier tube, D = iris diaphragm, L = lens, PH = 50 μm pinhole, SF = spectral filter, F = Filament, and S = substrate.

The schematic of our CRDS setup is shown in Figure 1. An excimer-laser-pumped dye laser (Lambda-Physik) working with coumarin 440 was used as the pulse source. The pulses are 15 ns long with 0.18 cm^{-1} linewidth. After frequency doubling in a BBO crystal with an Inrad Autotracker, the 214 nm pulse was shaped with the system of pinholes and lenses to match approximately the TEM_{00} transverse mode of the optical cavity. The quasi-hemispherical optical

cavity was 62 cm long with a flat entrance mirror and a 2 m curvature concave back mirror. The mirrors were coated by Lightning Optical Corp. and achieved 98.9 % reflectivity at 213.9 nm, as determined directly by the ring-down time τ_0 of the empty cavity. The TEM_{00} cavity mode has approximately a cylindrical form with a waist of 0.5 mm in diameter.

The light transmitted through the back mirror of the cavity was collected by a photomultiplier (PMT) and the PMT signal as a function of time was recorded on an HP 54510A digitizing oscilloscope with 2 ns temporal resolution. The ring-down waveforms digitized on the oscilloscope were transferred to a PC computer, averaged, and the ring-down time τ was obtained from a real-time computer fit. The CH_3 absorbance is then obtained from Eq. (1) below.

$$\alpha l_s = \frac{t_r}{2}\left(\frac{1}{\tau} - \frac{1}{\tau_0}\right) \tag{1}$$

where τ_0 is the empty cavity ring-down time, α is the sample absorption coefficient, and L_s is the sample length. In our experiment L_s is assumed to be equal to the filament length. With α thus determined, the absolute number density of the absorber, n, may be ascertained via knowledge of the cross-section σ and the relation $\alpha = \sigma$ n.

The hot-filament reactor consists of a 5-way stainless steel cross 4 inches in diameter. A two-stage mechanical pump (E2M40, Edwards) is used to evacuate the chamber to the minimum pressure of $4x10^{-3}$ Torr. The chamber is filled with 20 Torr mixture of H_2 with 0.5 % of CH_4 flowing at a rate of 100 sccm. The tungsten filament is 20 mm long and 200 μm in diameter. It is positioned horizontally inside the chamber using two tungsten posts, 4 cm long and 1.5 mm in diameter, mounted on water-cooled copper electrodes. The filament is resistively heated with dc current to a brightness temperature of 2300 K, which is monitored with a disappearance pyrometer (Pyro Micro-Optical Pyrometer). The substrate is made of a molybdenum strip (4 mm x 20 mm x 250 μm) and is resistively heated. The substrate temperature is monitored with a K Type thermocouple which is welded to the rear surface. The front surface is scratched with 10 μm diamond paste. The reactor condition is stabilized for at least 12 hours before CRDS measurement are performed.

RESULTS

We have applied CRDS to measure methyl radical concentration in two different reactor geometries. In the first geometry, the axis of the circulating CRDS beam is aligned parallel to the filament, and is translated in the plane defined by the filament and the substrate's long axis. In this manner, absorbance as a function of lateral position is mapped out, and converted to absolute number density as described above. Figure 2 shows the spatial profiles of the CH_3 number density (absorbance) measured in this manner within the hot-filament reactor at two different substrate temperatures. In this study, the filament temperature is held constant at 2300 K, the total pressure is 20 Torr, and the gas mixture is 0.5% CH_4 in H_2 flowing from left to right at a flowrate of 100 sccm. One can observe that the concentration of methyl radicals falls rapidly with increasing distance from the filament, and that the methyl radical concentration increases significantly at the higher substrate temperature. It is interesting to note that the methyl concentration well upstream of the filament is strongly influenced by the substrate temperature, possibly due to an overall increase in the reactor temperature field and hence methyl radical production. One can also observe that for the 900 °C substrate condition that the peak methyl

concentration occurs at a distance away from the filament (approx. 2 mm). This peaked result agrees qualitatively with the behavior of the CH_3 REMPI signal as a function of a distance from the filament reported by Ota and Fujimori,[6] but the peak CH_3 concentration we find is two orders of magnitude higher than their estimate. Goodwin, Glumac, and Corat[8] also measured spatial profiles of the CH_3 REMPI signal in the hot-filament reactor; however, their data do not extend to positions close to the filament and cannot be directly compared with our observations.

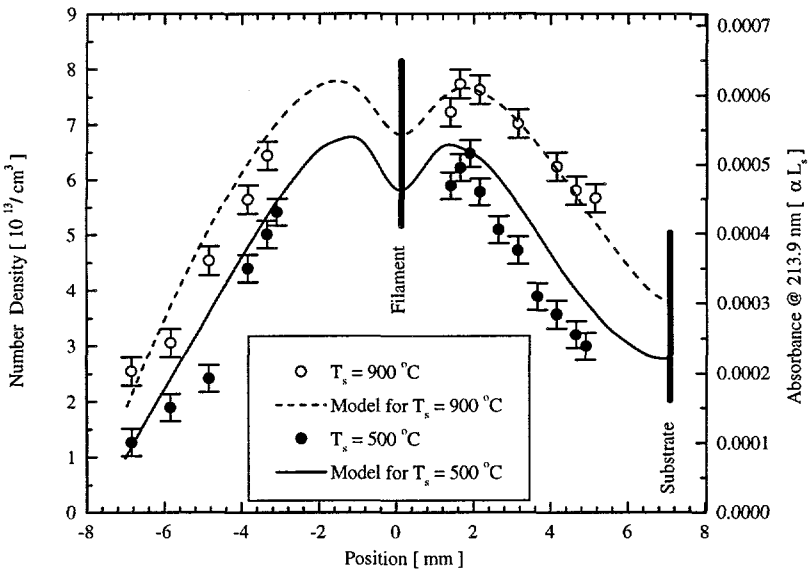

Figure 2. Spatial profiles of the measured CH_3 number density (absorbance) within the hot-filament reactor.

Figure 2 also shows the methyl radical concentration profile predicted by the two-dimensional model of Mankelevich et al.[24] for the same reactor conditions probed experimentally. In this two-dimensional model conservation equations for species, mass, momentum, and energy are solved including molecular and thermal diffusion, along with chemistry for 15 species via 38 reversible reactions. Temperature "slips" at the filament and substrate surface are prescribed from a separate Monte Carlo simulation. The largest uncertainty in this model is the production rate of atomic hydrogen at the filament surface. The results of the model prediction are in good agreement with the experimental measurements both in shape and relative magnitude for the two cases presented. Deviation of the model and experimental data near the substrate in the case of T_{sub}=500 °C is most likely due to the sensitivity of methyl radical production to the local gas temperature.

McMaster and coworkers[25] discuses the limitations of many of the HFCVD diamond reactor models. One-dimensional models are limited in their ability to account for the true geometry of reactors, often neglecting reactor walls or other surfaces that effect the gas phase composition and leaving out the three dimensional character of diffusion. Proper modeling of the hot filament environment requires sufficient knowledge of the interaction of the hot filament surface with the gas phase. Despite the fact that much of the gas phase species are dominated by the effects of the hot-filament, little work has been done to assess this interaction.

The second reactor geometry investigated was aimed at understanding the production mechanism of the methyl radical near the filament surface. In this geometry the substrate was removed to provide an axisymmetric temperature and concentration field about the axis of the

filament. (The slight asymmetry introduced by the slow motion of gas through the reactor has been demonstrated in our reactor to be negligible in an experiment where the flow direction was reversed). The axis of the CRDS circulating beam was then aligned perpendicular to the axis of the filament at its approximate midpoint. In this configuration the CRDS beam was translated away from the filament, effectively probing various chords of the axisymmetric methyl radical field. With the aid of an Abel transform[26] these lateral data can be converted into a profile of the absolute methyl radical concentration as a function of radial distance from the filament. Results of this study are shown in Figure 3 for a 200 μm diameter filament at a temperature of 2400 K, a reactor pressure of 20 torr, and a mixture of 0.5% CH_4 in H_2.

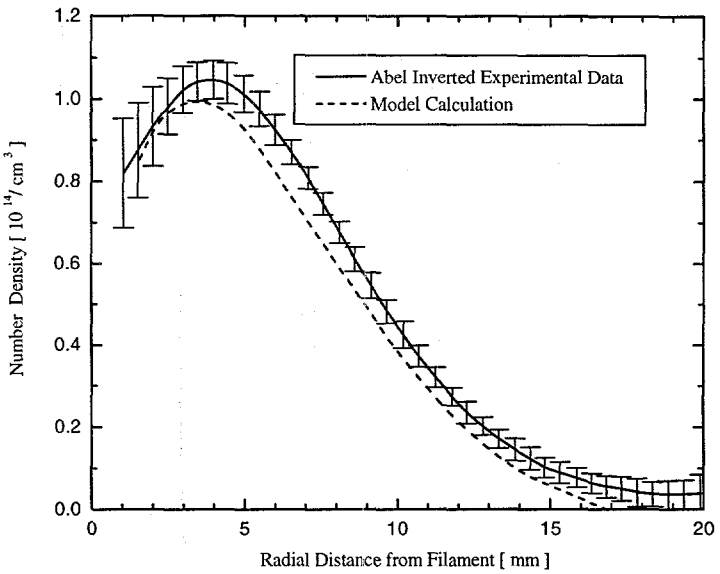

Figure 3. Radial distribution of the CH_3 concentration near the hot filament obtained by the Abel inversion of the absorbance profile.

In Figure 3 we can see the methyl radical concentration peak at approximately 10^{14} molecules/cm^3 some 4 mm radially away from the filament surface. Also shown in Figure 3 is a simplified model calculation for this geometry and operating parameters performed by Roozbehani,[27] who solved the one-dimensional radial species conservation equation including molecular and thermal diffusion (assuming that the production of methyl is spatially constant). The results of this model are in good agreement with the experimental data (although Roozbehani suggests that the *absolute* agreement is probably fortuitous) and the calculation yields a similar decay and location of the maximum in the methyl radical concentration.

To understand this off-filament peak of the methyl radical concentration we must consider several mechanisms. First, atomic hydrogen is produced at the filament surface, while CH_4 (and CH_3) are converted to C_2H_y species at the filament surface[28, 29] - hence the filament is an effective sink for these hydrocarbons. Secondly, thermal (or Soret) diffusion of species within the reactor causes the lighter components such as atomic hydrogen to diffuse toward hotter regions of the reactor, while heavier species such as methane diffuse toward the cooler regions[27, 30]. This creates a tendency toward thermal segregation of the mixture components, with atomic hydrogen remaining near the filament, and methane moving away from the filament. Finally, the production of methyl radical is dominated by the fast reaction: $H+CH_4 \leftrightarrow H_2 + CH_3$, which is in partial equilibrium throughout most of the reactor and strongly links the methyl radical

concentration field to that of atomic hydrogen and methane. The net effect of these various mechanisms is to create a rising concentration of atomic hydrogen as one approaches the filament, a declining concentration of methane towards the filament, and a production mechanism for methyl that swings from production to destruction depending upon whether hydrogen rises faster than methane declines. Roozbehani has shown in 2D simulations of a HFCVD reactor,[27] that without the effect of Soret diffusion the balance shifts towards a monotonic rise in production as one approaches the filament (hence no peak in methyl concentration), and that by including Soret diffusion the experimentally measured peak in methyl concentration is accurately predicted.

Methyl radical number density measurements were also taken very near the substrate surface (within ~0.5 mm) as a function of both substrate and filament temperature. Results of those measurements are shown in Figures 4 and 5 respectively. In both cases the reactor pressure was 20 Torr with a mixture of 0.5% CH_4 in H_2 flowing at a rate of 100 sccm, and the substrate prepared by operating at diamond growth conditions of T_f = 2300 K , T_s = 900 °C for approximately 12 hours. In Figure 4, the filament temperature was held at 2300 K while the substrate temperature was increased from 600 °C to 1200 °C. The power to the substrate was increased after each data point by increments of approximately 50 °C and allowed to stabilized for 10 minutes before the next point was taken. One can see an approximately linear increase in the near surface methyl radical concentration with increasing substrate temperature. This is in qualitative agreement with the results of Corat and Goodwin[7] for the near surface region, although our data does not extend to high enough temperature to confirm their observed high temperature roll-off in methyl concentration. Our observed activation energy of the near surface radical concentration, based on substrate temperature, is 4.2 ± 0.2 kcal/mol. This value agrees with the value reported by Corat and Goodwin.[7]

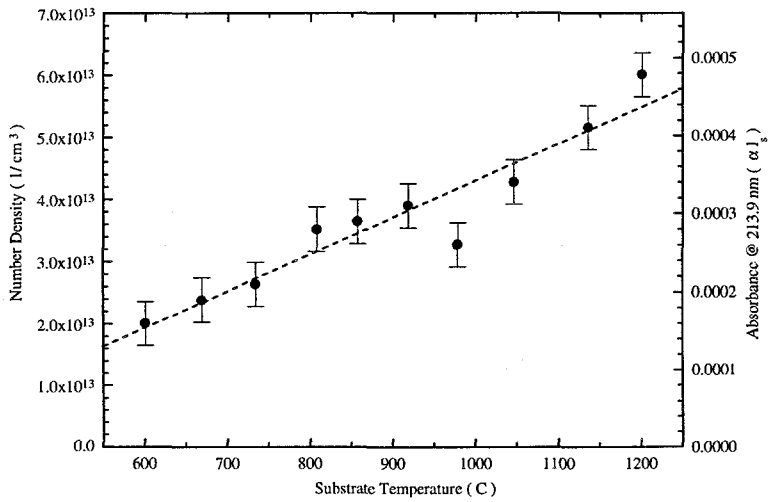

Figure 4. Variation of the CH_3 number density (absorbance) near the substrate surface (within ~0.5 mm) as a function of substrate temperature.

In Figure 5, the substrate temperature was held at 900 °C while the filament temperature was increased from approximately 2000 K to approximately 2550 K. We observe the near surface methyl concentration to first increase strongly with increasing filament temperature, and then to saturate somewhat above 2400 K. This strong increase is in qualitative agreement with the

REMPI measurements of Corat and Goodwin,[7] but we do not observe a decrease in methyl concentration above 2300 K as evident in their measurements. Our data trends do, however, compare favorably to the model predictions of Kondoh et al.[14]

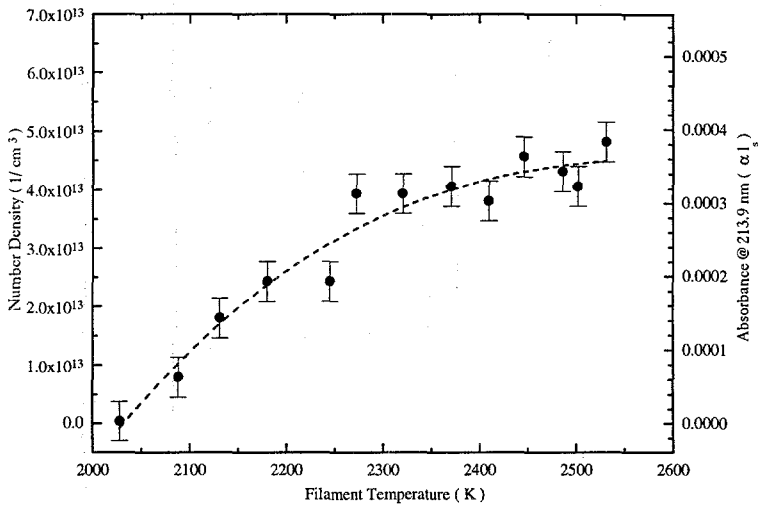

Figure 5. Variation of the CH_3 number density (absorbance) near the substrate surface (within ~0.5 mm) as a function of filament temperature.

ACKNOWLEDGMENTS

The authors would like to acknowledge contributions by E.H. Wahl and by the companion research program of Prof. R.N. Zare, with Dr. D. Aderhold and B.A. Paldus (DOE Grant #DE-FG03-92ER14304)

REFERENCES

1. S. J. Harris and L. Robbin Martin, "Methyl versus acetylene as diamond growth species," *Journal of Materials Research*, vol. 5, pp. 2313-19, 1990.
2. M. Frenklach, "Monte Carlo simulation of diamond growth by methyl and acetylene reactions," *Journal of Chemical Physics*, vol. 97, pp. 5794-802, 1992.
3. S. S. Lee, D. W. Minsek, D. J. Vestyck, and P. Chen, "Growth of diamond from atomic hydrogen and a supersonic free jet of methyl radicals," *Science*, vol. 263, pp. 1596-8, 1994.
4. F. G. Celii, P. E. Pehrsson, H. t. Wang, and J. E. Butler, "Infrared detection of gaseous species during the filament-assisted growth of diamond," *Applied Physics Letters*, vol. 52, pp. 2043-5, 1988.
5. E. Villa, J. A. Dagata, J. Horwitz, D. Squire, and M. C. Lin, "Methyl radical formation from filament pyrolysis of acetylene and acetylene/hydrogen mixtures within quartz tubes," *Journal of Vacuum Science & Technology A (Vacuum, Surfaces, and Films)*, vol. 8, pp. 3237-40, 1990.
6. N. Ota and N. Fujimori, "In situ detection of methyl radicals in filament assisted diamond growth environment by resonance ionization spectroscopy," presented at the Advanced in New Diamond Science and Technology, MYU, Tokyo, Japan, 1994.
7. E. J. Corat and D. G. Goodwin, "Temperature dependence of species concentrations near the substrate during diamond chemical vapor deposition," *Journal of Applied Physics*, vol. 74, pp. 2021-9, 1993.
8. D. G. Goodwin, N. G. Glumac, and E. J. Corat, "Optical detection of CH_3 during diamond chemical vapor deposition," presented at the SPIE conference on laser techniques for state-selected and state-to-state chemistry, Los Angeles, CA, 2124, 1994.

9. M. A. Childs, K. L. Menningen, P. Chevako, N. W. Spellmeyer, L. W. Anderson, and J. E. Lawler, "Detection of CH_3 during CVD growth of diamond by optical absorption," *Physics Letters A*, vol. 171, pp. 87-9, 1992.

10. H. Toyoda, M. A. Childs, K. L. Menningen, L. W. Anderson, and J. E. Lawler, "Ultraviolet spectroscopy of gaseous species in a hot filament diamond deposition system when C_2H_2 and H_2 are the input gases," *Journal of Applied Physics*, vol. 75, pp. 3142-50, 1994.

11. W. L. Hsu, "Mole fractions of H, CH_3, and other species during filament-assisted diamond growth," *Applied Physics Letters*, vol. 59, pp. 1427-9, 1991.

12. S. J. Harris and A. M. Weiner, "Methyl radical and H-atom concentrations during diamond growth," *Journal of Applied Physics*, vol. 67, pp. 6520-6, 1990.

13. E. Kondoh, T. Ohta, T. Mitomo, and K. Ohtsuka, "Effect of gas-phase composition on the surface morphology of polycrystalline diamond films," *Diamond and Related Materials*, vol. 3, pp. 270-6, 1994.

14. E. Kondoh, T. Ohta, T. Mitomo, and K. Ohtsuka, "Experimental and calculational study on diamond growth by an advanced hot filament chemical vapor deposition method," *Journal of Applied Physics*, vol. 72, pp. 705-11, 1992.

15. D. Romanini and K. K. Lehmann, "Ring-down cavity absorption spectroscopy of the very weak HCN overtone bands with six, seven, and eight stretching quanta," *Journal of Chemical Physics*, vol. 99, pp. 6287-301, 1993.

16. P. Zalicki and R. N. Zare, "Cavity ring-down spectroscopy for quantitative absorption measurements," *Journal of Chemical Physics*, vol. 102, pp. 2708-17, 1995.

17. A. O'Keefe, J. J. Scherer, A. L. Cooksy, R. Sheeks, J. Heath, and R. J. Saykally, "Cavity ring down dye laser spectroscopy of jet-cooled metal clusters: Cu_2 and Cu_3," *Chemical Physics Letters*, vol. 172, pp. 214-18, 1990.

18. T. Yu and M. C. Lin, *Journal of the Americal Chemical Society*, vol. 115, pp. 4371, 1993.

19. G. Meijer, M. G. H. Boogaarts, R. T. Jongma, D. H. Parker, and A. M. Wodtke, "Coherent cavity ring down spectroscopy," *Chemical Physics Letters*, vol. 217, pp. 112-16, 1994.

20. A. O'Keefe and D. A. G. Deacon, "Cavity ring-down optical spectrometer for absorption measurements using pulsed laser sources," *Review of Scientific Instruments*, vol. 59, pp. 2544-51, 1988.

21. J. Gardiner, W.C., S. M. Hwang, and M. J. Rabinowitz, "Shock tube and modeling study of methyl radicals in methane oxidation," *Energy & Fuels*, vol. 1, pp. 545-549, 1987.

22. S. M. Hwang, M. J. Rabinowitz, and W. C. Gardiner, Jr., "Recombination of methyl radicals at high temperatures," *Chemical Physics Letters*, vol. 205, pp. 157-62, 1993.

23. P. Zalicki, Y. Ma, R. N. Zare, E. H. Wahl, J. R. Dadamio, T. G. Owano, and C. H. Kruger, "Methyl radical measurement by cavity ring-down spectroscopy," *Chemical Physics Letters*, vol. 234, pp. 269-74, 1995.

24. Y. A. Mankelevich, A. T. Rakhimov, and N. V. Suetin, "Two-dimensional model of reactive gas flow in a diamond film CVD reactor," *Diamond and Related Materials*, vol. 4, pp. 1065-8, 1995.

25. M. C. McMaster, W. L. Hsu, M. E. Coltrin, and D. S. Dandy, "Experimental measurements and numerical simulations of the gas composition in a hot-filament-assisted diamond chemical-vapor-deposition reactor," *Journal of Applied Physics*, vol. 76, pp. 7567-77, 1994.

26. C. O. Laux, "Optical Diagnostics and Radiative Emission of Air Plasmas," Ph.D. Thesis, Stanford University, (1993).

27. B. Roozbehani, "Electrodeposition of Carbon from Aqueous Solutions and Experimental and Modeling Studies of CVD Diamond Film Synthesis," Ph.D. Thesis, Case Western Reserve University, (1996).

28. S. J. Harris and A. M. Weiner, "Pressure and temperature effects on the kinetics and quality of diamond films," *Journal of Applied Physics*, vol. 75, pp. 5026-32, 1994.

29. S. J. Harris, "Private Communication," , 1995.

30. S. Chapman and T. G. Cowling, *The mathematical theory of non-uniform gases*. Cambridge: Cambridge University Press, 1960.

PLASMA DEPOSITION OF ADVANCED MATERIALS

D. Kolman, H.C. Chen, J. Heberlein, E. Pfender

Department of Mechanical Engineering
University of Minnesota
Minneapolis, MN 55455

ABSTRACT

Plasma coating technology has the distinct advantage that a large variety of materials can be deposited at high rates. In this paper we describe two examples where the characteristics of the plasma process offers the potential of improving the economics of specific manufacturing processes. The deposition of diamond can be improved by using liquid precursors, however, it has become evident that scaling required a more detailed process understanding. A 3-dimensional model is described which provides insight into the details of the chemical and physical processes leading to the film deposition. The conclusion derived from this model is that the liquid has to reach the substrate boundary layer to increase deposition rates. In the second example, a newly developed process is described which has the potential for a more economical manufacture of solid oxide fuel cells. The three layers of the cell are all plasma deposited in the same chamber at rapid rates. The individual layers, in particular the yttria stabilized zirconia electrolyte layer, have been tested for performance, and complete cells obtained with this new process are presently being tested.

INTRODUCTION

More efficient and more environmentally friendly energy utilization has strongly increased the demand for multifunctional uses of materials in manufacturing. These demands can be met by specialty coatings on the most suitable structural material. In addition, the use of suitable coatings allows the selection of a wider variety of structural materials some of which may offer specific advantages. While several coating processes have been developed for aerospace applications, their use in large scale manufacturing requires improved economics, which includes increased reliability and process yield and high deposition rates. This is particularly true for coatings based on thermal plasma technology, such as plasma spraying and thermal plasma CVD. A detailed process understanding is necessary to optimize the process, develop adaptive controls, and design equipment tolerant to uncontrolled process variations.

In this paper we report on two developments in plasma coating technology having the goal of increasing process economics by making use of the special characteristics of the thermal plasma. The first effort is devoted to the improvement of the deposition rate of diamond coatings to make this type of coating economically attractive for tools or heat sinks. A process model is described for a diamond deposition process involving liquid precursors, a technology which has demonstrated experimentally to allow deposition at the highest rates. The second part is devoted to the description of a new coating process developed for the economical preparation of solid oxide fuel cells (SOFC's). While SOFC's have proven to be an attractive source of electrical energy, their costs are so far too high to allow them to find wide spread use. Reduction of their manufacturing costs will have a significant impact on the way energy will be supplied in the future.

DIAMOND DEPOSITION WITH LIQUID PRECURSORS

Description of Problem and Approach

We have reported previously the results of experiments in which some of the highest diamond growth rates reported in the literature have been achieved [1]. In these experiments an organic liquid, e.g. ethanol or acetone, has been injected into an argon-hydrogen plasma jet in a counterflow arrangement. Growth rates of approximately 1 mm/hr have been obtained. However, while we further developed this process to make full use of this newly discovered effect, inconsistencies in the observed results have been encountered. To resolve the question of what process variables are responsible for the high growth rate, a model has been developed for predicting the diamond growth in a reactor closely simulating the experimental deposition reactor. Figure 1 shows the experimental deposition reactor in the side injection mode, and Fig. 2 shows the computational domain of the model. In this figure, the plasma torch is at the top of the figure with the jet pointing downward towards the substrate. Two atomization probes are positioned opposing each other 2 mm above the substrate close to the substrate edge. The model is fully three dimensional and combines several submodels:
(1) A fluid dynamics model describing the turbulent plasma jet;
(2) a liquid atomization model describing the formation of the liquid droplets in front of the injection probes with hydrogen as the atomizing gas;
(3) a droplet evaporation model describing the transport of the liquid droplets by the atomization gas into the plasma jet, the heating of the droplets, evaporation of the liquid and dissociation of the resulting gas molecules;
(4) a chemical kinetics model describing the chemical reactions in the entire domain;
(5) a surface chemistry model describing the diamond growth on the substrate.
The argon - hydrogen plasma gas mixture is flowing into the domain with a specified temperature and velocity profile at the nozzle exit which is the inlet of the calculation domain. The profiles are adjusted to reflect measured values of the total enthalpy flow and total mass flow rate.

Model Formulation

Details of the model formulation have been given elsewhere [2]. The gas phase fluid dynamics model consists of a set of conservation equations for mass, momentum and energy, but there is mass addition due to evaporation of the droplets. In addition, species

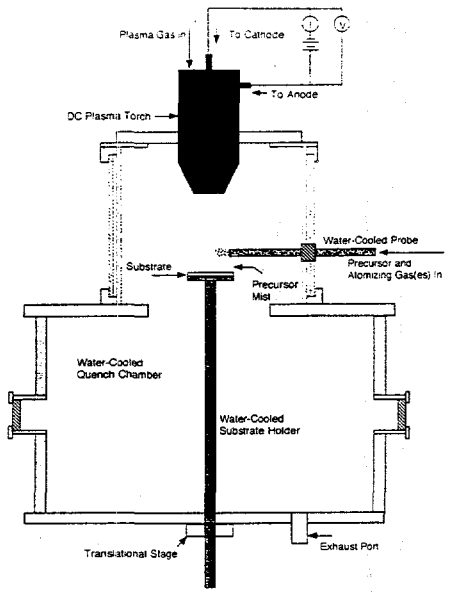

Fig. 1 Schematic of experimental set-up

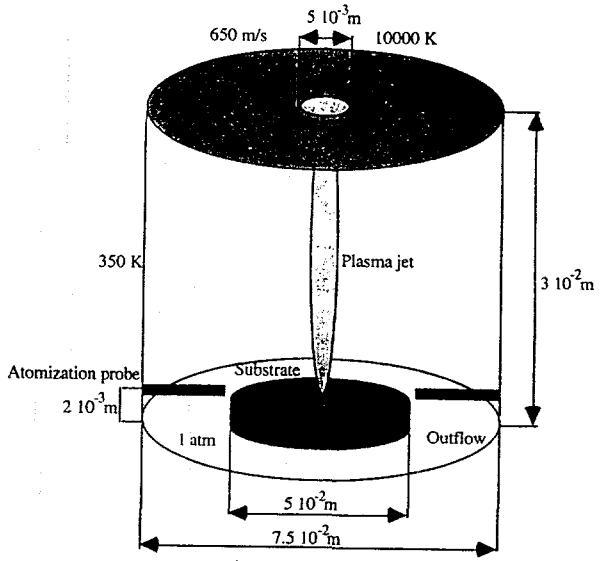

Fig. 2 Computational domain for liquid injection model

conservation has to be considered. The phase change also results in an additional term in the energy equation. The atomization model and the calculation of the Sauter mean diameter follows the formalism given by [3]. The vaporization model considers both limitations, the first imposed by the vapor transfer number being determined by the vapor concentration at the droplet (subcritical vaporization), and the second by the energy conservation at the droplet (critical vaporization).

The model will perform the following computational steps:

1) Computation of gas phase flow, enthalpy and concentration fields for the major chemical species using the SIMPLER code [4]. The chemical species boundary conditions are given in terms of species fluxes due to surface chemistry. Surface chemistry is a function of gas phase composition and surface fractional coverage, the latter being updated simultaneously with the gas phase iteration. Laminar transport properties as well as gas phase and gas phase - surface chemical kinetics are evaluated using the code CHEMKIN [5]. Turbulent transport properties are calculated from a k-ε model.

(2) Liquid atomization is calculated and the droplet trajectories are determined; vaporization and energy fluxes are computed.

(3) Vaporization and energy fluxes are introduced as source terms into the gas phase equations, and chemical species fields and surface chemistry are recomputed.

Model Results

Solutions have been obtained for different precursor chemicals - ethanol and acetone, and methane as comparison, for different injection probe locations, different droplet sizes, different atomization gas flow rates, and different amounts of hydrogen in the plasma jet. Figure 3 shows calculated droplet trajectories for two different atomization processes. The left figure indicates the standard droplet formation process, while in the right hand figure the

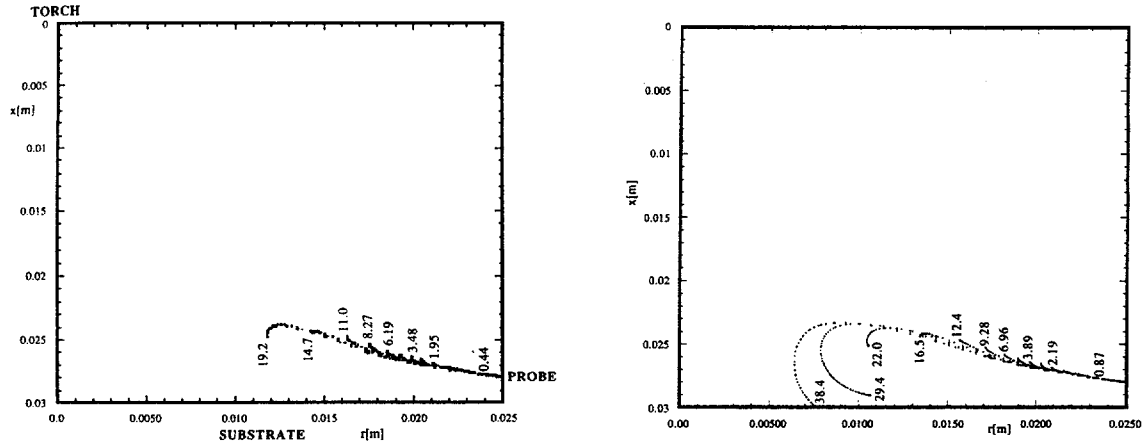

Fig. 3 Calculated droplet trajectories for two different atomization mechanisms

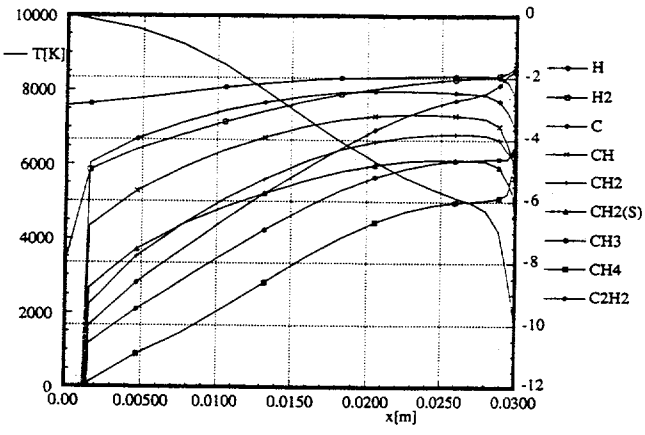

Fig. 4 Calculated axial temperature and species mass fraction distributions (log scale)

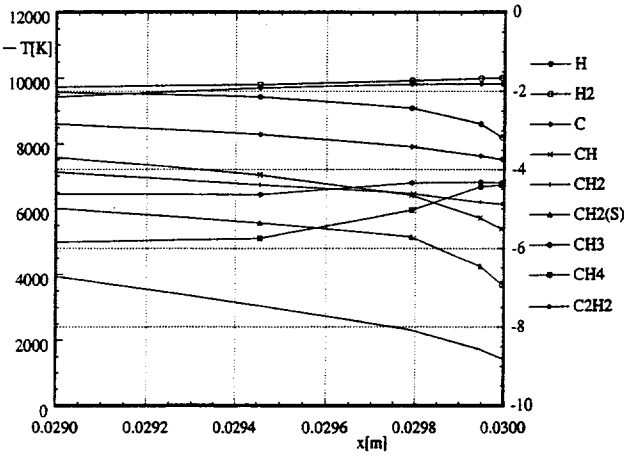

Fig. 5 Calculated axial temperature and mass fraction distributions (log scale) in the boundary layer

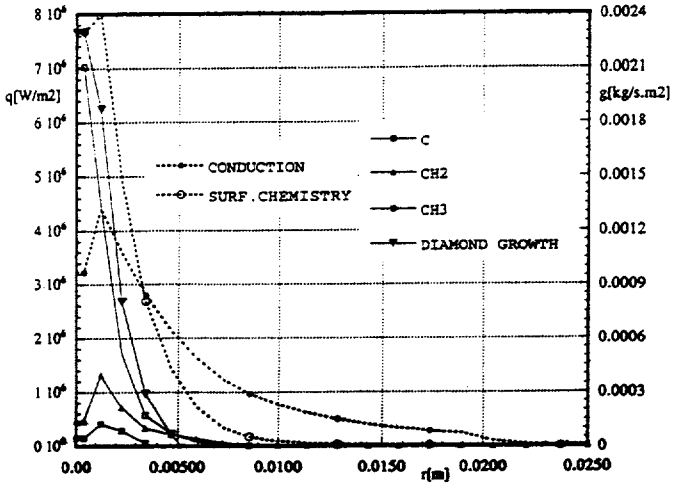

Fig. 6 Radial heat flux and diamond deposition rates

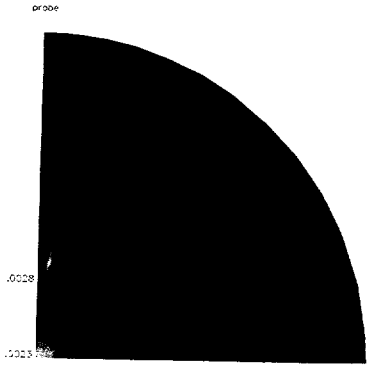

Fig. 7 Diamond growth distributions with large droplet injection

droplet size is doubled to artificially account for some droplet agglomeration following the initial atomization process. The droplets exit from the probe tip on the right hand side, and depending on their initial size, have trajectories of different lengths before they evaporate. The initial droplet diameter is indicated with the trajectory. It is interesting to notice that for this case the droplets evaporate before they enter the substrate boundary layer, and the vapor is carried by the plasma gases into a recirculation region from where they enter the plasma jet and are transported to the substrate. Figure 4 shows the axial distributions of the temperature and mass fractions of several species on the centerline between the plasma torch nozzle and the substrate. The temperature drops gradually from the peak value of 10000 K at the nozzle exit to a value of about 4500 K at the edge of the boundary layer. The mass fraction distributions show that the atomic hydrogen mole fraction stays high up to the edge of the boundary layer, and that the mass fraction of atomic carbon also remains high. Figure 5 shows the details of the axial distributions over the last millimeter in the boundary layer above the substrate. A drop of atomic hydrogen is noticeable accompanied by an increase in ethylene and a decrease of atomic carbon. However, the atomic hydrogen mass fraction remains sufficiently high to have an abundance of atoms for surface passivation, and the number of carbon atoms remains sufficiently high to make this species the dominant deposition precursor. Figure 6 shows the radial distributions of the contributions of thermal conduction and chemical reactions (hydrogen recombination) to the total substrate heat flux, as well as the total diamond growth rate and the contribution to the total growth by atomic carbon, by CH_2 and by CH_3. It is apparent that chemical reactions dominate the substrate heat flux, and atomic carbon is the precursor species with the strongest contribution to diamond growth.

There is little difference in the results obtained for different precursors, indicating that for this case of complete droplet evaporation the carbon containing molecules are dissociated to a sufficient degree so that boundary layer recombination is determining the diamond growth behavior. However, there are droplets reaching the boundary layer (see Fig. 3). These droplets evaporate when coming into contact with the substrate which is at a temperature of 1273 K, and the area where this evaporation takes place has a very high density of dissociation products of the hydrocarbon precursors. The consequence is a very high local deposition rate over a relatively small area, with CH_3 being the dominant deposition precursor. This is shown in Fig. 7 which depicts a quarter of the substrate with the growth areas indicated. Besides the area of diamond growth in the center of the substrate due to the precursors transported into the jet via the recirculation, there is an area of high growth visible closer to the tip of the injection probe.

These results let us conclude that the cause for the experimentally observed high deposition rates is an improved mass transport provided by the liquid droplets, and that chemistry influences this growth only insofar as the dissociation products contain oxygen and/or OH radicals which assure that little graphite is deposited.

PLASMA COATINGS FOR SOLID OXIDE FUEL CELLS

Description of Problem and Approach

In solid oxide fuel cells, the fuel (e.g. hydrogen) supply is separated from the supply of the oxidant (oxygen) by a impermeable membrane which allows only oxygen ions to diffuse from the oxygen supply side to the fuel. Thus, reaction of the hydrogen and the oxygen to form water is accompanied by the deposition of a negative charge on the hydrogen

supply side, and electricity can be generated without going through a thermal power plant cycle. A typical fuel cell is built such that a porous layer consisting of a cermet, e.g. nickel - zirconia, allows the hydrogen to flow to the electrolyte membrane, typically yttria stabilized zirconia (YSZ), where it reacts with the oxygen ion which diffused through the membrane. The oxygen reaches the other side of the membrane, the "cathode side," by flowing through a porous lanthanum - manganese oxide perovskite layer. The YSZ membrane allows diffusion of oxygen ions at elevated temperatures of approximately 900°C. The requirements for the three fuel cell layers are: the cermet anode has to have sufficiently high electrical conductivity to allow the current to flow to the load connection, and has to have good resistance to corrosion by hydrogen and steam. The perovskite cathode has to be electrically conducting as well, and be resistant to oxidation attack. The electrolyte has to have good dielectric properties and should be impermeable to the hydrogen.

Fuel cells of this type have been successfully operated for many years, however, their manufacturing costs have been relatively high. We have developed plasma deposition processes which allow the preparation of a fuel cell at a rapid rate. Central to this development has been a new process for deposition of a dense YSZ layer at a rate of about 50 μm/min. This deposition is performed in a reactor developed under a previous DOE sponsored project, the triple torch plasma reactor [6]. To increase the economy of the SOFC preparation process, the deposition of all three layers has been performed in this reactor, allowing the principal parts of a cell to be built in less than one hour.

Description of Experiment

The triple torch plasma reactor consists of a controlled atmosphere chamber with three plasma torches mounted on its top flange (see Fig. 8). These torches are powered independently and their position can be adjusted independently. The jets of these torches combine to form an enlarged plasma region into which the deposition precursors are injected as powder, liquid droplets or vapors. This arrangement allows a good mixing of the reactants with the plasma and efficient heating by the plasma.

For the deposition of the high density YSZ layer, a new process has been developed in which a fine YSZ powder is injected into the plasma, completely melted and partially vaporized. The deposition mechanism has been observed with a telemicroscope, and the hybrid vapor - liquid deposition nature of the process has been confirmed by these observations. The deposition parameters are shown in Table 1.

Table 1 Typical parameters for the low pressure center injection deposition process

Power input	12 kW per torch
Plasma gas	Ar : 16 slm, H_2 : 0.35 slm for each torch
Chamber pressure	100 Torr
Powder feed rate	8 g/min
Carrier gas	Ar : 5 slm
Stand-off distance	150 mm

For deposition on a substrate with large pores, it has been necessary to deposit an intermediate layer, such as a conventional atmospheric pressure sprayed YSZ layer with low porosity. However, this intermediate layer is not necessary when the anode layer has been deposited in the triple torch reactor. For the deposition of this anode layer, a mixture of

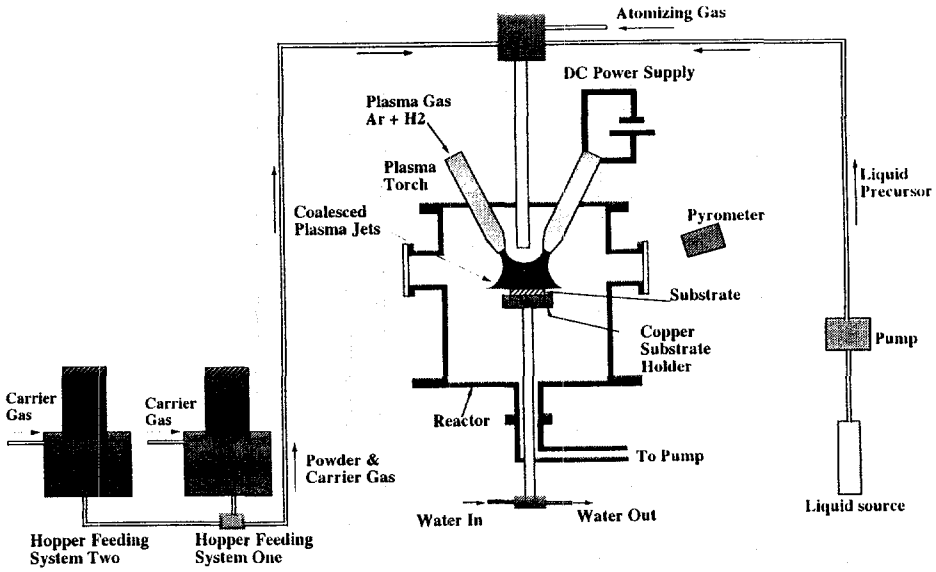

Fig. 8 Schematic of triple torch reactor

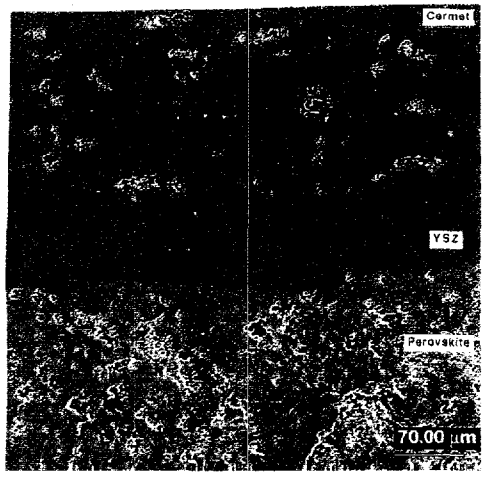

Fig. 9 Micrograph of solid oxide fuel cell cross section as prepared in the triple torch reactor

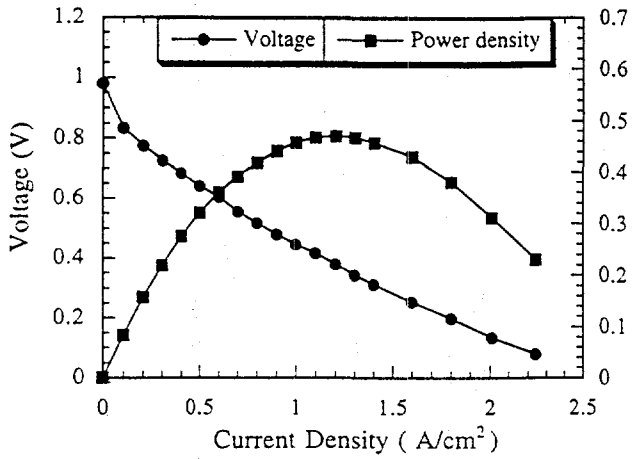

Fig. 10 V - I characteristic and power density for fuel cell prepared with new YSZ electrolyte deposiiton process

nickel oxide with standard size YSZ powder has been injected into the triple torch, and deposition at higher pressure resulted in a porous layer. The cermet is then formed by reduction of the nickel oxide in the hydrogen atmosphere during the initial operation of the fuel cell at a temperature of about 900°C.

For the deposition of the cathode layer, a thermal plasma CVD process has been chosen. Nitrate solutions of manganese and lanthanum have been injected through an atomizing probe as fine liquid spray into the plasma. Use of liquid precursors has two advantages, namely it is possible to adjust the optimal composition for the formation of the perovskite layer by adjusting the concentrations of the liquid solution, and the use of nitrates avoids the high cost of perovskite powders.

Film Deposition Results

Deposition of the electrolyte YSZ layer with the newly developed center injection low pressure hybrid plasma spray - vapor deposition process (CILPS) has resulted consistently in very dense layers with porosities lower than 1%, at rapid rates (about 50 μm/min). Films deposited on sintered cermet substrates with a thickness of about 40 μm have been evaluated for performance as a fuel cell dielectric, and open circuit voltages of 1 V or above have been obtained with maximum power densities of approximately 0.5 W/cm^2. Figure 9 shows a micrograph of the polished cross section of the triple layer fuel cell, indicating the high density of the YSZ electrolyte layer, as well as the uniformity of the NiO - YSZ cermet layer. The difference in the microstructure of the center injection deposited YSZ layer compared to regularly plasma sprayed YSZ layers is seen on micrographs of a fracture surface of a structure consisting of an atmospheric pressure plasma sprayed intermediate layer between the porous cermet substrate and the high density electrolyte layer. The CILPS deposited layer shows a very fine grain structure with translamellar type of fracture indicating the liquid sintering which takes place during deposition. X-ray diffraction of the layer shows a single (400) peak indicating that the YSZ layer possesses a cubic phase structure.

Figure 10 shows performance evaluation graphs of a cell constructed of a sintered cermet with the CILPS electrolyte layer and a metallic grid cathode. The open circuit voltage of O.97 V and the maximum power density of 0.47 W/cm^2 are respectable initial performance indicators. Cells consisting of three layers all deposited in the triple torch reactor in a single multistep process are presently under evaluation.

A problem of the multilayer fuel cell is that strong stresses develop particularly at the interfaces between the porous cermet and the dense YSZ layers during the thermal cycling of the cell operation. These stresses can lead to cracks which reduce the performance characteristics. The fuel cell manufacture in the triple torch plasma reactor allows grading of the composition of the layers thus reducing the stress formation. Experiments with deposition of graded films are in progress.

CONCLUSIONS

Thermal plasma processes offer special advantages for the deposition of some specific materials, including deposition at high rates and with a variety of feedstock material. The consequences are improved process economics. We have demonstrated that diamond deposition rates can be enhanced significantly by the use of liquid precursors, and a model of

the process details shows that this is accomplished when the deposition precursors are transported in the liquid phase directly into the boundary layer. This process description has been obtained by the formulation of a unique model which treats the variety of microscopic processes in a three-dimensional formulation. The development of this model will be of benefit for the description of other plasma based multi-phase processes.

The challenging task of forming a high density dielectric electrolyte layer for solid oxide fuel cells at a rapid rate has been accomplished by developing a new type of deposition process. Characterization of existing CVD or spray deposition processes has shown the shortcomings of these traditional approaches - either too low deposition rates or insufficient density requiring too thick layers. The new process makes use of plasma equipment with unique characteristics developed under previous DOE sponsorship. The triple torch plasma reactor lends itself to the deposition of high density yttria stabilized zirconia films at rapid rates using center injection into the plasma at reduced pressures. Furthermore, this plasma reactor is suited to integrating the preparation processes for all the components of the SOFC. This presents an opportunity for improving the economics for the fuel cell manufacture thus increasing the attractiveness of this electric energy source.

ACKNOWLEDGMENT

This research has been supported by the Department of Energy, Office of Basic Energy Sciences. We also acknowledge the collaboration of Professor T. Yoshida for the functional evaluation of the fuel cell under the sponsorship of the Japanese NEDO agency.

REFERENCES

1. E. Pfender, q.Y. Han, T.W. Or, Z.p. Lu, and J. Heberlein, "Rapid synthesis of diamond by counterflow liquid injection into an atmospheric-pressure plasma jet," *Diamond and Related Materials*, 1, 127-133 (1992).

2. D. Kolman, J. Heberlein, and E. Pfender, A Three-Dimensional Two-Phase Model for Thermal Plasma Chemical Vapor Deposition with Liquid Feedstock Injection," *Plasma Chemistry and Plasma Processing*, 18, 73-89 (1998).

3. F.W. Bracco, "Structure of high-speed full cone sprays," in Recent Advances in the Aerospace sciences, C.Casci, ed., Plenum, New York (1985).

4. S.V. Patankar, "Numerical Heat Transfer and Fluid Flow," Hemisphere Publishing Corp., New York (1980).

5. R.J. Kee, F.M. rupley, J.A. Miller, "Chemkin-II: A Fortran Chemical Kinetics Package for Analysis of Gas Phase Chemical Kinetics," Sandia National Laboratories, September 1989.

6. R.M. Young, E. Pfender, "A Novel Approach for Introducing Particulate Matter Into thermal Plasmas: the Triple Cathode Arc," Plasma Chem. Plasma Process., 10, 167-188 (1990).

7. H.C. Chen, J. Heberlein, and T. Yoshida, "Preparation of Films for Solid Oxide Fuel Cells by Center-Injection Low Pressure and Atmospheric Plasma Spraying," to be published in Proc. ITSC, May 1998.